Mineralium Deposita (2021) 56:1543–1562
https://doi.org/10.1007/s00126-020-01029-w

ARTICLE

Geology and genesis of the Shalipayco evaporite-related Mississippi Valley-type Zn–Pb deposit, Central Peru: 3D geological modeling and C–O–S–Sr isotope constraints

Saulo B. de Oliveira[1] · Craig A. Johnson[2] · Caetano Juliani[1] · Lena V. S. Monteiro[1] · David L. Leach[3] · Marianna G. N. Caran[1]

Received: 6 April 2020 / Accepted: 17 November 2020 / Published online: 7 January 2021

Abstract

The Shalipayco Zn–Pb deposit, in central Peru, is composed of several stratabound orebodies, the largest of which are the Resurgidora and Intermedios, contained in carbonate rocks of the Upper Triassic Chambará Formation, Pucará group. Petrography suggests that a single ore-forming episode formed sphalerite and galena within vugs, open spaces, and fractures. Three-dimensional (3D) geological modeling has allowed division of the Chambará Formation into four members (Chambará I, II, III, and IV) that better define lithological controls on sulfide formation. Diagenetic replacement of evaporite minerals with the organic matter (OM) presence likely generated secondary porosity and H_2S accumulation by bacterial sulfate reduction (BSR), providing ground preparation for the later Zn–Pb mineralizing event. The least-altered host rocks have C–O isotope compositions of 1.8 ± 0.1‰ (VPDB) and 29.9 ± 2.1‰ (VSMOW), respectively, within the Triassic marine carbonate ranges. Early dolomite contains lighter C–O composition (1.1 ± 0.9 and 23.8 ± 2.9‰, respectively) consistent with OM decomposition during burial diagenesis. Post-mineralization calcite has still lighter C–O composition (− 5.1 and 13.3‰, respectively), suggesting meteoric water that had migrated through organic-rich strata. The strontium isotopes of Mitu group basalts (0.709654–0.719669) indicate it as a possible, but not the unique source of strontium and probably of other metals. Highly negative sulfide sulfur isotope values (− 23.3 to − 6.2‰ (VCDT)) indicate a major component of the ore sulfur derived ultimately from BSR. However, multiple lines of evidence suggest that preexisting H_2S underwent thermochemical redox cycling prior to ore formation. The influx of hot metalliferous brines to dolomitized zones containing trapped H_2S is the preferred model for ore deposition at Shalipayco.

Keywords Evaporite-related MVT deposits · C, O, S, Sr isotopes · Pucará group · Chambará formation · Shalipayco · 3D geological modeling

Introduction

The Shalipayco Zn–Pb deposit is located in the central highlands of Peru, 170 km northeast of Lima and 35 km southeast of the city of Cerro de Pasco (Fig. 1). The deposit consists of stratabound orebodies hosted in Late Triassic to Early Jurassic carbonate rocks of the Pucará group. Ore sulfide outcrops have been identified along a NW strike length of approximately 12 km in the deposit area. Near-surface ore was exploited in small underground mines during the 1970s. The Shalipayco deposit comprises several distinct orebodies. The most important are the Resurgidora and Intermedios levels, which contain most of the known resources and are the focus of this work. Also discussed are the sulfide exposures at the Eddy vein occurrence, which are structurally controlled, although subsurface extensions have not been confirmed by drilling.

Editorial handling: K. Kelley

✉ Saulo B. de Oliveira
sauloboliveira@hotmail.com

[1] Instituto de Geociências, Universidade de São Paulo, São Paulo, São Paulo 05508-080, Brazil

[2] US Geological Survey, MS 963, P.O. Box 25046, Denver, CO 80225, USA

[3] Center for Mineral Resources Science, Department of Geology and Geological Engineering, Colorado School of Mines, Golden, CO 80401, USA

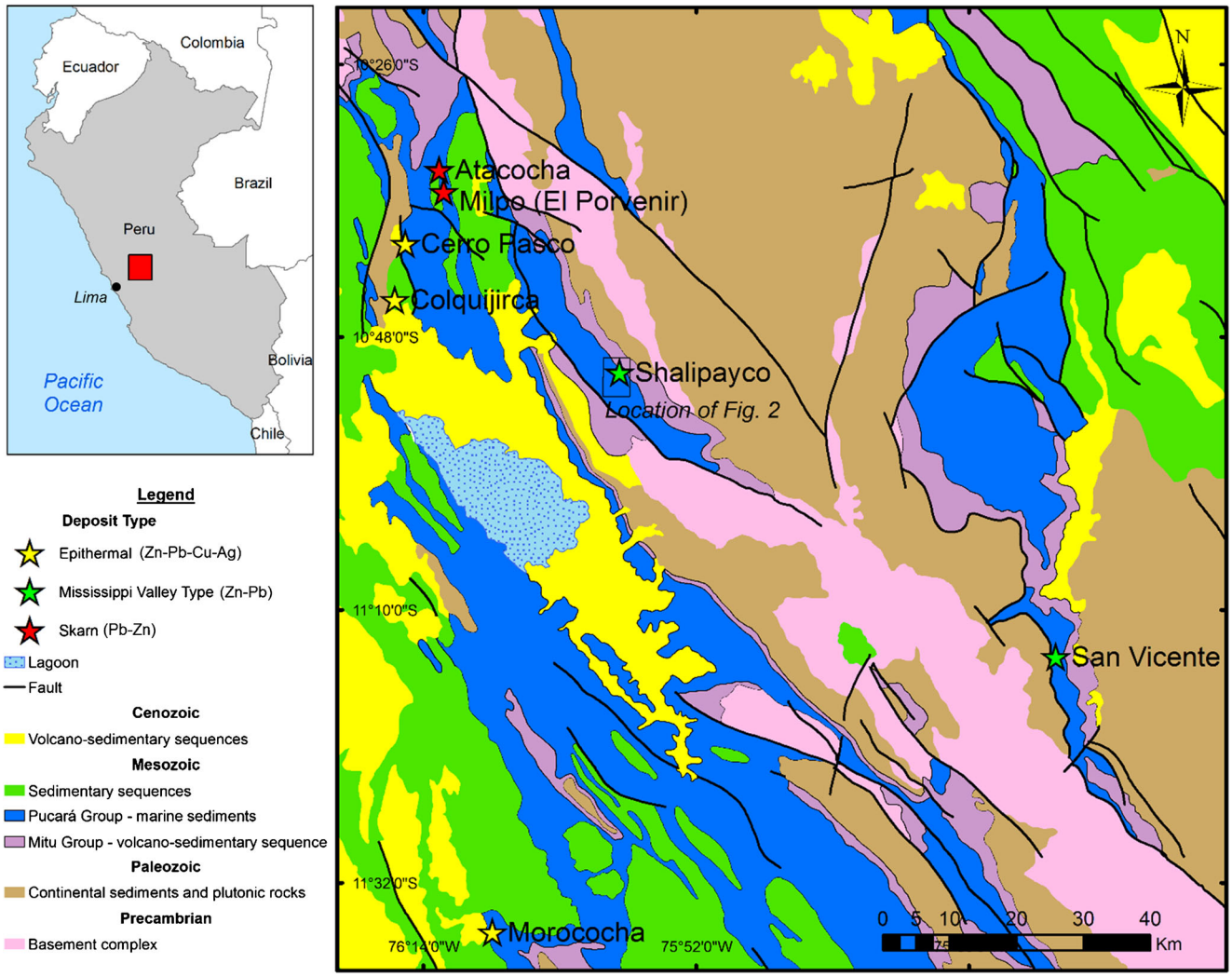

Fig. 1 Geologic map of central Peru (simplified after INGEMMET 1999) showing the location of the Shalipayco deposit and several other deposits hosted by the Pucará group. Map location is shown in inset. Box enclosing Shalipayco is the area shown in Fig. 2

Over a broader geographic area in central Peru (Fig. 1), Pucará group carbonate rocks host other Zn–Pb deposits including San Vicente (Fontboté and Gorzawski 1990), Florida Canyon, about 1000 km north of Shalipayco (Basuki et al. 2008; de Oliveira et al. 2019a; de Oliveira et al. 2019b; de Oliveira and Saldanha 2019; de Oliveira et al. 2020), Cerro de Pasco (Baumgartner et al. 2008; Rottier et al. 2018a; Rottier et al. 2018b), Colquijirca (Bendezú and Fontboté 2009), Atacocha and Milpo (Gunnesch and Baumann 1984), and Morococha (Catchpole et al. 2015a; Catchpole et al. 2015b). Some of these deposits are within magmatic-hydrothermal districts with a large variety of mineralization styles, including skarn, carbonate-replacement, and high- and intermediate-sulfidation epithermal associated with porphyry copper systems (Sillitoe 2010).

Aspects of the Shalipayco deposit have been discussed by Fontboté (1990), Fontboté et al. (1990), Gunnesch et al. (1990), Soler and Lara (1990), and Moritz et al. (1996). However, detailed geological descriptions have not yet been published. Due to regional geological characteristics, the Shalipayco deposit could be a distal carbonate-replacement deposit that is part of a large magmatic-hydrothermal system similar to some of the abovementioned districts in the vicinity. On the other hand, the Shalipayco Zn–Pb deposit may represent a Mississippi Valley-type (MVT) deposit, as assumed by previous authors (Fontboté 1990; Fontboté et al. 1990; Soler and Lara 1990; Moritz et al. 1996), similar to the San Vicente Zn–Pb deposit (Fontboté and Gorzawski 1990).

This paper presents new observations of the Shalipayco deposit based on the geological understanding developed by exploration geologists who worked on the project including Tuanama (2016). This study also addresses the genesis of the deposit with an evaluation of a MVT versus distal carbonate-replacement origin possibly associated with large magmatic-hydrothermal systems (Sillitoe 2010) that formed the nearby base metals districts. The discussion of the genetic model is

based on new geological observations, three-dimensional (3D) geological modeling, whole-rock geochemistry, C–O–S, and Sr isotope data.

Regional geologic setting

In the central Andes, tectonic movements of the South American plate produced three different physiographic features: (1) the Western Cordillera, which includes the magmatic arc above the subduction zone; (2) the Eastern mountain range that represents a region of uplift; and (3) the intervening Andean Altiplano. The geology of the Andes is the result of three separate geodynamic events during the Proterozoic, from the Paleozoic to Early Triassic, and the Andean cycle from the Late Triassic to Holocene time (Benavides-Cáceres 1999). The third event, the Andean cycle, began with the Late Triassic opening of the Atlantic Ocean (Mégard 1984, 1987; Benavides-Cáceres 1999). During this period, the back-arc zone in what is now central Peru experienced extension, generating a series of horsts and grabens. Volcaniclastic and clastic sequences of the Triassic Mitu group (Spikings et al. 2016) formed in the early stages of extension. These rocks have thicknesses of 800 to 1500 m, and consist of conglomerates, sandstones, basalts, and polymictic breccias with andesitic fragments (Noble et al. 1978).

Extension and subsidence during rifting produced a Mesozoic marine basin, the Pucará Basin (Mégard 1987; Benavides-Cáceres 1999). Located in north-central Peru, the Pucará Basin is bounded on the east by the Guyana Shield and west by the Peruvian Altiplano (Rosas et al. 2007). The basin represents the first marine transgression of the Andean cycle covering sediments of the Mitu group. The marine strata consist of shallow platform deposits, such as limestone and dolostone, fine-grained organic rich clastic rocks, and evaporites.

Pucará group sediments were deposited between the Late Triassic and Early Jurassic (Mégard 1968; Szekely and Grose 1972). A Norian age for the early stages of deposition is based on fossils (Sánchez 1995) and zircon U-Pb ages for volcanic ash layers within the sequence (Schaltegger et al. 2008; Wotzlaw et al. 2014). Three formations comprise the Pucará group, each distinguished by lithotype, fossil content, facies, and geochemistry (Mégard 1968). The basal unit, the Chambará Formation, consists predominantly of dolostone and limestone, with chert nodules or centimeter-thick highly fossiliferous chert bands (Mégard 1968). Rosas et al. (2007) suggested that the Chambará Formation sediments were derived from a carbonate platform developed during the transition from fault-controlled rifting to post-rift regional subsidence. The considerable variation of the unit thickness, from 25 to 1170 m, is considered to be a consequence of changes in the rate of subsidence (Rosas et al. 2007). The overlying Aramachay Formation consists of calcareous and fetid black shales with bituminous and occasional silty beds containing ammonites (Ritterbush et al. 2015). Though poorly exposed, this unit is laterally homogeneous and is thought to reflect a stable platform environment (Rosas et al. 2007). The uppermost member of the Pucará group, the Condorsinga Formation, is composed predominantly of limestone with dolostone occurring locally in the basal portions reflecting a shallow platform environment. This unit differs from the Chambará Formation in that chert and dolostone occurs only in the basal parts of the sequence. Lenses with pseudomorphs after evaporite minerals suggest that second-order basins or lagoonal environments developed leading to hypersaline conditions. Ammonites constrain the age of this formation to latest Sinemurian through Toarcian time, a span of ca. 25 Ma (Mégard 1968). Condorsinga Formation rocks rarely crop out due to Andean structural inversion and erosion (Rosas et al. 2007).

In Peru, the dominant structural Andean trend is northwest (Fig. 1). The Shalipayco deposit is located on the Sub-Andean thrust and fold belt (Mégard 1984) characterized by southwest-dipping thrust faults. In the vicinity of the deposit, the local faults have directions ranging from north-northeast, north, and north-northwest (e.g., Eddy vein) (Fig. 2). The temporal relation between the faults is still not entirely clear, but they are conditioned (not offset) by the regional northwest thrust faults.

Base metals deposits hosted in the Pucará group in Central Peru

In the central region of Peru, where the Shalipayco deposit is located, numerous base metal deposits are hosted in the Pucará group. Four magmatic-hydrothermal districts composed of epithermal, carbonate-replacement, skarn, and porphyry deposits stand out. The Morococha district, approximately 80 km southwest of Shalipayco (Fig. 1), is characterized by the giant Toromocho porphyry Cu-Mo deposit in the center with peripheral Zn–Pb–Ag–Cu veins and replacements that cover an area of approximately 50 km^2 (Catchpole et al. 2015a; Catchpole et al. 2015b). All multistage intrusions in the Morococha district are calc-alkaline in composition with ages ranging from 9.3 to 5.7 Ma (Catchpole et al. 2015a). The Cerro de Pasco-Colquijirca districts, approximately 40 km northwest of Shalipayco (Fig. 1), feature large epithermal polymetallic (Zn–Pb–Cu–Ag) deposits, commonly termed Cordilleran deposits (Baumgartner et al. 2008; Bendezú and Fontboté 2009; Rottier et al. 2018a; Rottier et al. 2018b). Mineral deposits within these two districts are associated with dacitic diatreme-dome complexes; in the Cerro de Pasco region, ages of the igneous rocks are 15.4 to 15.1 Ma (Baumgartner et al. 2008) whereas ages in the Colquijirca district are between 12.4 and 12.12 Ma (Bendezú et al.

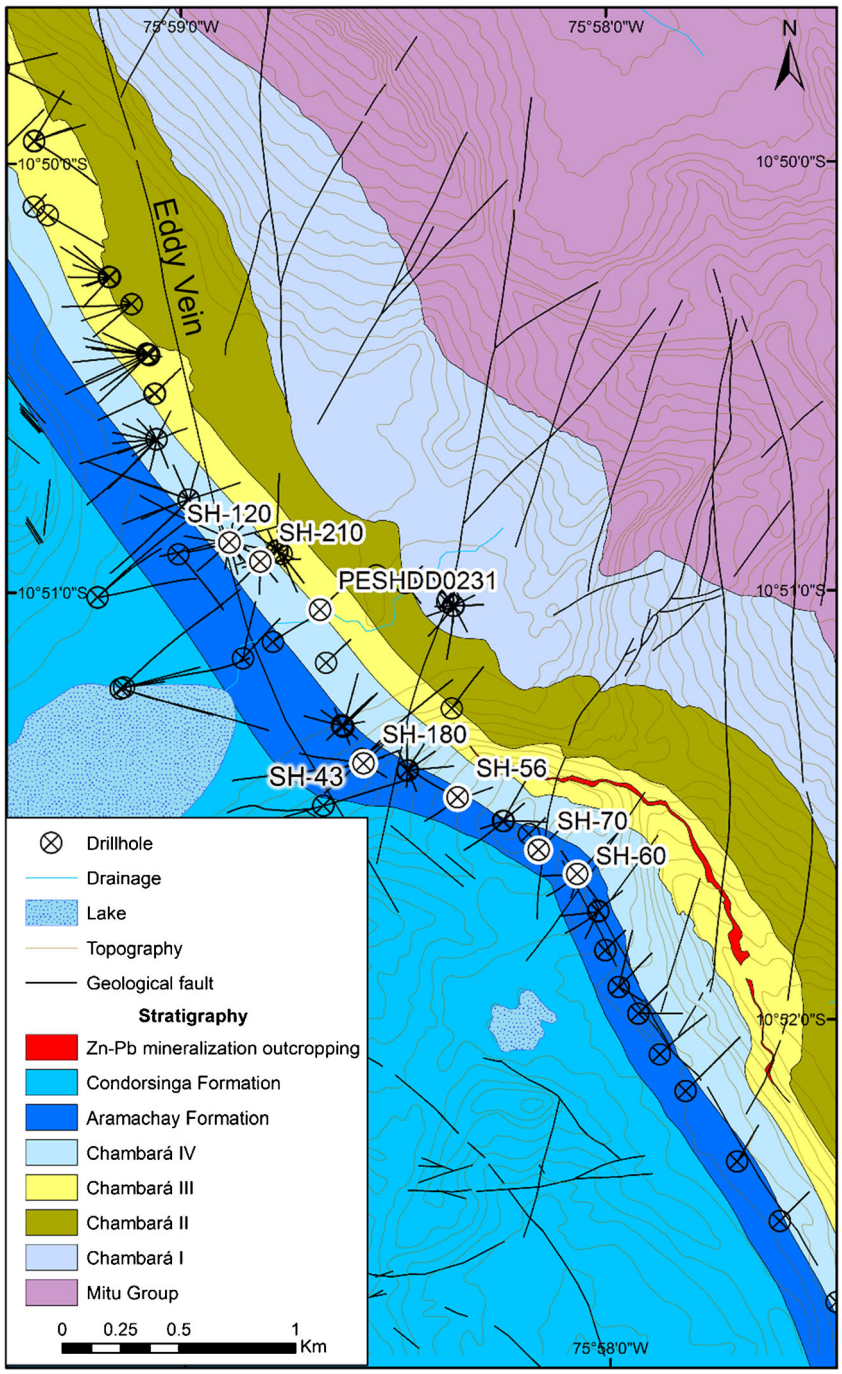

Fig. 2 Geologic map showing subdivisions of the Chambará Formation in the vicinity of the Shalipayco deposit and drillhole locations. The SH-43 drillhole location overlaps the SH-180 location on the given map scale

2003). A few kilometers to the north are the skarn Pb-Zn deposits of Atacocha and Milpo (El Porvenir), which are also related to dacitic magmatism of uncertain age (Gunnesch and Baumann 1984).

The San Vicente MVT Zn–Pb deposit of assumed Eocene and Miocene age (Moritz et al. 1996; Spangenberg et al. 1999; Badoux et al. 2001) is located approximately 75 km southeast of Shalipayco (Fig. 1). The Florida Canyon Zn–Pb MVT deposit, about 1000 km north of Shalipayco, is also hosted in carbonates and evaporites of the Pucará group. The deposit is considered to have formed in Upper Cretaceous time (Reid 2001; Basuki et al. 2008; de Oliveira et al. 2019b; de Oliveira et al. 2020).

Samples and procedures

We collected 101 samples from seven drillholes spatially distributed throughout the entire deposit (SH-56, SH-60, SH-70, SH-120, SH-180, SH-210, and PESHDD0231) and an eighth

drillhole that extends stratigraphically lower and cuts all the lithological units (SH-43) (Fig. 2). The samples were examined in hand specimen and in thin section using a Leica DM750P optical microscope equipped with both transmitted and reflected light. Thin section billets were treated with potassium ferrocyanide and Alizarin-S in order to differentiate calcite, dolomite, and iron carbonates.

Fluid inclusions were studied in doubly polished thin sections using an Olympus BX51 microscope in the Fluid Inclusion Laboratory at the Colorado School of Mines, USA. Because the inclusions are small (less than 5 μm in diameter), it was impossible to obtain accurate microthermometric measurements (Goldstein and Reynolds 1994).

Concentrations of Ag, As, Ba, Be, Bi, Cd, Co, Cr, Cu, Hg, In, Mn, Mo, Ni, Pb, Sb, Sr, Ti, V, W, and Zn were obtained for 20,538 drill core whole-rock samples from the Nexa Resources database. The samples comprised half the core split vertically in intervals of approximately 1 m, so the data represent continuous sections. The analyses were performed by ALS Chemex, Toronto, Canada, using an inductively coupled plasma atomic emission spectrometer (ICP-AES) after fine crushing (to 70 wt.% < 2 mm), pulverizing (to 85 wt.% < 75 μm), and four-acid digestion, using a combination of nitric, perchloric, and hydrofluoric acid with a final dissolution stage using hydrochloric acid. A complete description of analytical methods is available on the ALS Chemex home page (www.alsglobal.com).

Sulfur isotope analyses of sphalerite, galena, pyrite, and barite were obtained in laboratories of the Geology, Geophysics, and Geochemistry Science Center, US Geological Survey, Denver, CO, USA, following the procedures of Johnson et al. (2018). Isotopic compositions are reported in delta notation relative to Vienna Cañon Diablo troilite (VCDT). For carbon and oxygen isotope analyses, a Dremel 3000 drill device with a 2-mm tungsten carbide tip was used for selective sampling of different carbonate generations. Some samples were whole rocks (limestone), whereas others were specific minerals (e.g., late calcite). Sample powders were forwarded to the Stable Isotope Laboratory, University of São Paulo, Brazil (LIESP-USP), for analysis. Approximately 100 μg of powder was placed in a 12-ml vial, heated to a temperature of 72 °C, and flushed with helium gas. The isotope ratios were measured on CO_2 gas liberated on reaction with orthophosphoric acid using a Thermo Finnigan GasBench II coupled to a Delta V Advantage mass spectrometer. The results are reported in delta notation (in units of permil, ‰) relative to Vienna Peedee Belemnite (VPDB) for carbon and Vienna Standard Mean Ocean Water (VSMOW) for oxygen. Samples were analyzed in duplicate. The instrumental precision was ± 0.05‰ for $\delta^{13}C$ and ± 0.07 ‰ for $\delta^{18}O$ and accuracy was of ± 0.07 ‰ for $\delta^{13}C$ and ± 0.06 ‰ for $\delta^{18}O$.

Strontium isotope analysis was performed on three samples of limestone of Chambará Formation and three samples of basalt from Mitu group by thermal ionization mass spectrometry (TIMS) using a Thermo Triton mass spectrometer at the Centro de Pesquisas Geocronológicas, Universidade de São Paulo, Brazil (CPGeo-USP). The precision of a single analytical result is given as two-standard errors of the mean (2σ). Mean values for $^{87}Sr/^{86}Sr$ ratio of NBS-987 Sr standard analysis during November 2015 through August 2016 are 0.710237 ± 0.000014 (n = 200). The 87Sr/86Sr isotope ratios were normalized to $^{87}Sr/^{86}Sr = 0.1194$.

The 3D geologic model was generated using the Leapfrog Geo platform through implicit modeling techniques (Cowan et al. 2002; Cowan et al. 2003; Vollgger et al. 2015). The Shalipayco database contained 281 drillholes with a total of 89,500 m. The lithology data from logging were loaded in the software, and the surfaces were built using depositional contact surfaces type.

Results

Geology of the Shalipayco deposit

Textural and mineralogical characteristics of the Chambará formation host rocks at the deposit site

In the vicinity of the Shalipayco deposit, the Chambará Formation has been divided into four members, from base to top Chambará I, II, III, and IV (Figs. 2 and 3). The Chambará I member lies unconformably on the Mitu group (Fig. 3e) which, based on a few drillhole intersections, consists locally of polymorphic conglomerate, arkosic sandstone, and amygdaloidal volcanic rock (Fig. 3e). The Chambará I member with an average thickness of 320 m is dark gray lime mudstone to wackestone, locally with millimetric dark rounded clasts of chalcedony and small calcite grains (Fig. 3d). Sparry calcite replaces earlier carbonates and fills cavities. This unit is highly porous showing centimeter-size vugs. Dolomite fills fractures and locally contains disseminations of dark-brown sphalerite and pyrite. Late veins with sparry calcite infill are characteristic of the unit.

The Zn–Pb orebody of the Intermedios level is hosted by the Chambará II member (Fig. 3c) with an approximate thickness of 120 m comprising mainly porous gray dolostone composed of sparry planar dolomite crystals. Original sedimentary textures are typically obscured (Fig. 3c). Dolomitization was always accompanied by the deposition of late thin pyrite in the interstices of dolomite crystals. Late chalcedony replaces nodules. Medium-thick sparry calcite appears late in the paragenesis, crystallizing between dolomite crystals.

The Chambará III member hosts the Zn–Pb orebody of the Resurgidora level and is 80 m thick. This unit consists of beige, fetid, dolomitic boundstone with, in its uppermost strata, intercalations of micrite layers partially replaced by sparry

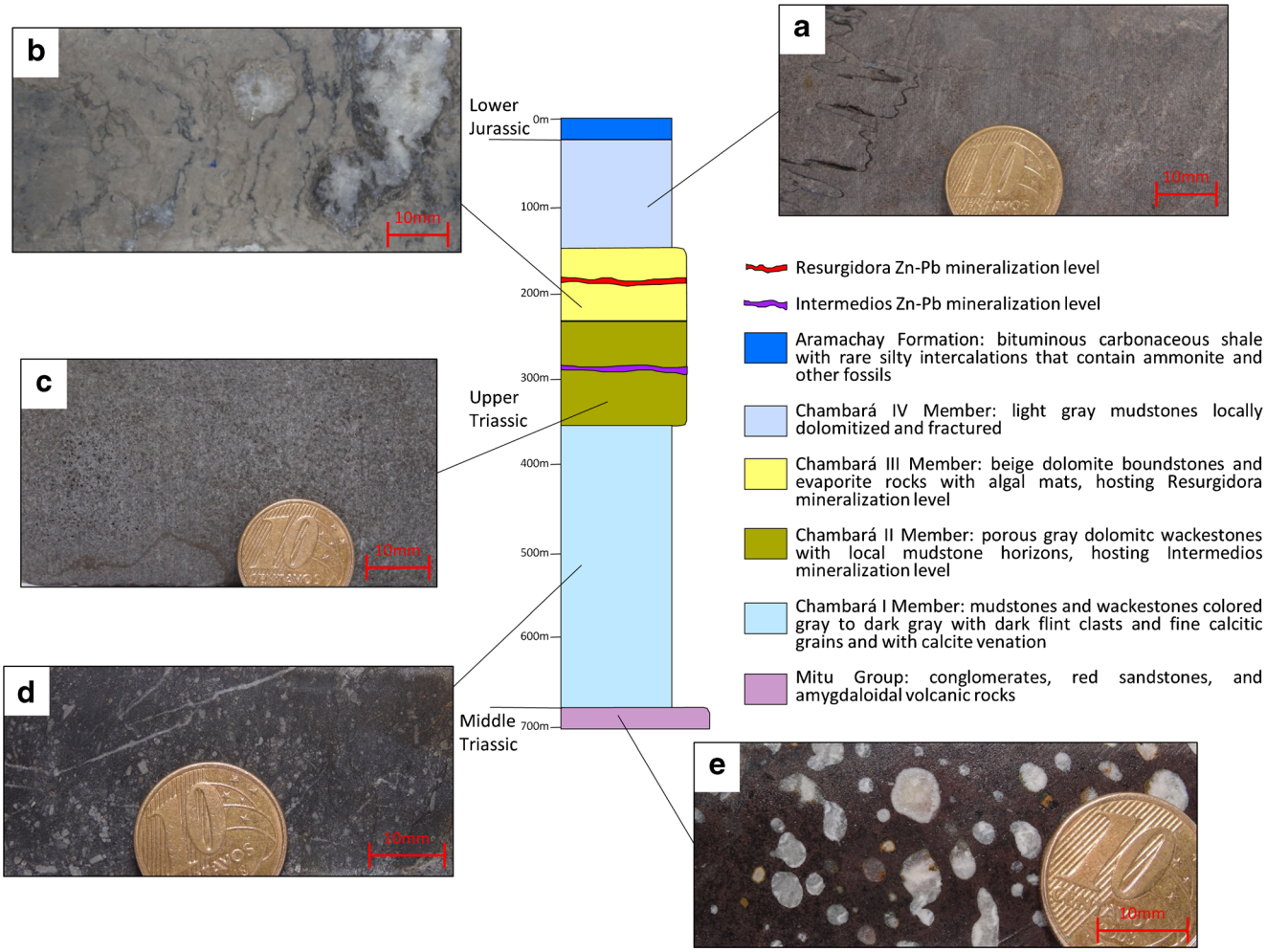

Fig. 3 Stratigraphic column in the vicinity of the Shalipayco deposit with photos of characteristic core samples: **a** SH-43-147.60: dark gray dolomitic mudstone with stylolites from Chambará IV member. **b** SH-180-189.70: beige dolomitic boundstone with calcite pseudomorphs after halite from Chambará III member. **c** SH-43-359.30: massive porous gray dolostone from Chambará II member. **d** SH-43-490.40: black massive packstone from Chambará I member. **e** SH-43-688.80: amygdaloidal andesite from Mitu group

dolomite and fine interlaminar micritic dolomite (Fig. 3b). Calcite nodules are common and are interpreted to be pseudomorphs after anhydrite. Late calcite and/or dolomite fill fractures. Stylolites are common and are generally filled with pyrite and organic matter. Bitumen occurs in pores and void fillings. Sulfides in these rocks include zoned dark-brown sphalerite, galena, fine- to medium-grained (~ 1 mm in diameter) pyrite, and fine-grained marcasite occurring as breccia matrix and as cavity and fracture fillings. Evaporite breccia textures can be observed in some locations, as described in the Florida Canyon deposit by de Oliveira et al. (2019b). Both Chambará II and III contain intercalations of partially dolomitized mudstone and wackestone with some preserved sedimentary textures and replaced evaporite horizons. The least-altered rocks consist of millimeter-sized ooids and oncoids with sub-concentric structures partially replaced by sparry dolomite. The matrix, when present, is micritic. Fine-grained dolomite fills vugs and is locally associated with barite crystals. Medium-grained (~ 0.5 mm diameter) sparry calcite is uncommonly associated with minor fluorite and occurs as the final stage of porosity fill and as breccia matrix.

The Chambará IV member has an approximate thickness of 130 m and is characterized by massive light gray lime mudstone (Fig. 3a) and wackestone with some fossils, especially pellets and bivalves, locally dolomitized and fractured. Local coarse-grained interlayers with greater porosity show local replacement of lime mud by dolomite. The replacement process resulted in the partial destruction of original sedimentary textures.

Two stratigraphic markers, both up to 10 m in thickness, are commonly used to recognize contacts between Chambará members. A fossiliferous horizon with crinoids, bivalves, and corals marks the top of Chambará I and the base of Chambará II, whereas a gray fetid dolomitic wackestone with sulfide, bitumen, and organic matter defines the top of Chambará III dolostones and the base of Chambará IV mudstones.

Tuanama (2016) presents additional subdivisions of the stratigraphy including 10 lithologic units and 5 horizons of sulfide occurrences. The lithologic controls for mineralization are summarized by Tuanama (2016). Dolostone horizons with well-developed porosity and permeability and replaced evaporite horizons are the most common hosts for stratabound Zn–Pb. The entire stratigraphy in the Shalipayco area is tilted with the dip direction of 225°/30°SW (Fig. 4); this dictates the direction of the Zn–Pb mineralized horizons. In the Shalipayco area, some minor intrusive rocks within the Pucará group (not represented on the map scale in Fig. 2) are described by Tuanama (2016) as metric late basalt dikes and small felsic domes emplaced in the Condorsinga Formation but with no spatial relationship with the Zn–Pb orebodies.

Evaporite horizons

A salt horizon is known below the Pucará group (Calderón et al. 2017a; Calderón et al. 2017b; Sempere and Cotrina 2018; Baby et al. 2019) and sabkha facies with evaporite minerals are well-known within the Pucará group itself (Benavides 1968; Fontboté and Gorzawski 1990). Textures within Shalipayco rocks contain evidence of former evaporite, porous dolostone, evaporite breccia, and pseudomorphs of evaporite minerals (Fig. 5). Porous dolostones are coarse, massive, and light brown to gray and have significant secondary porosity locally in the form of open pores (Fig. 5a) or sphalerite- or galena-filled pores (Fig. 5b). In less-altered boundstones, mudstones, and wackestones, acicular, fibrous, and radiating evaporite minerals are pseudomorphed by calcite (Fig. 5c). Evaporite breccias are dolomitic with local dark dolomite clasts set in a white sparry dolomite matrix or a chaotic mixture of dark and white dolomite generations (Fig. 5d, e), formed by the dissolution of evaporite horizons. Replacement of gypsum or anhydrite by sparry dolomite during burial diagenesis (Anderson and Garven 1987) generated open space due to the volume reduction that accompanies this replacement reaction making the breccia highly permeable. More detailed descriptions of porous dolostone and evaporite breccia are given by Leach and Song (2019) and de Oliveira et al. (2019b). Rounded calcite pseudomorphs after halite are present in beige dolomitic boundstone (Fig. 3a). Former evaporite horizons are present in both the

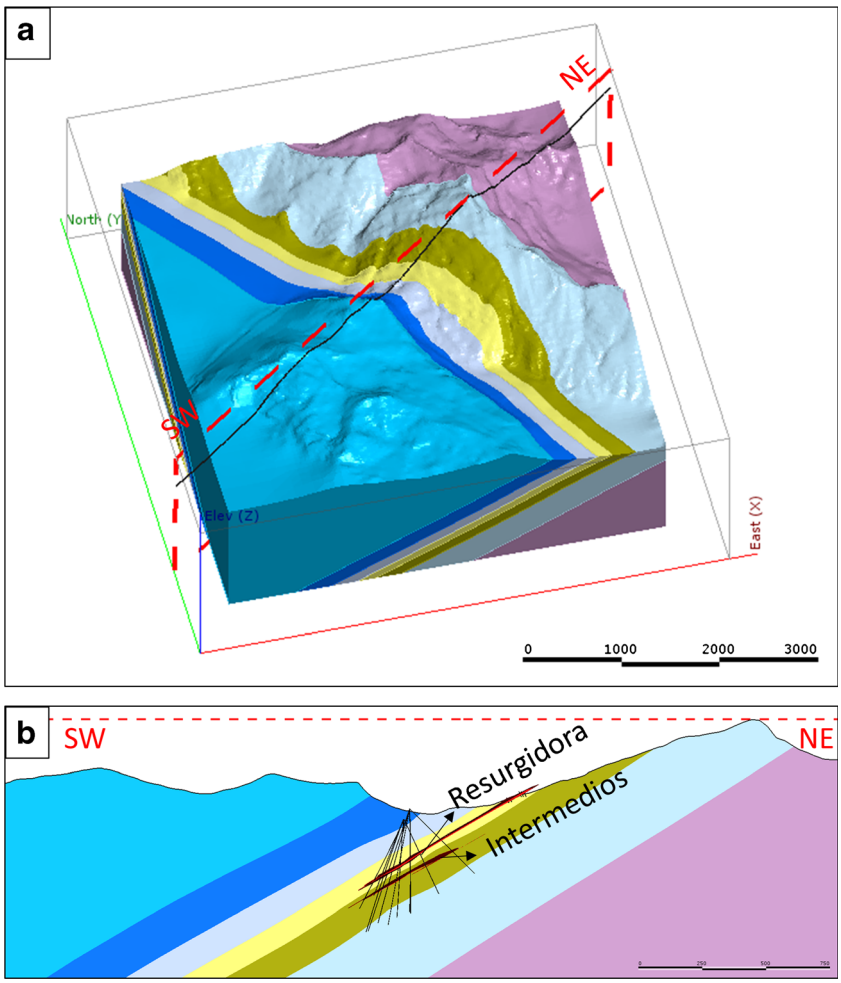

Fig. 4 **a** 3D geologic model of the Shalipayco deposit. **b** Geologic cross-section looking NW, perpendicular to the main dip direction (225°/30°SW), showing the Resurgidora and Intermedios layers. Colors correspond to the same lithologic units as in Figs. 2 and 3. Scale in meters

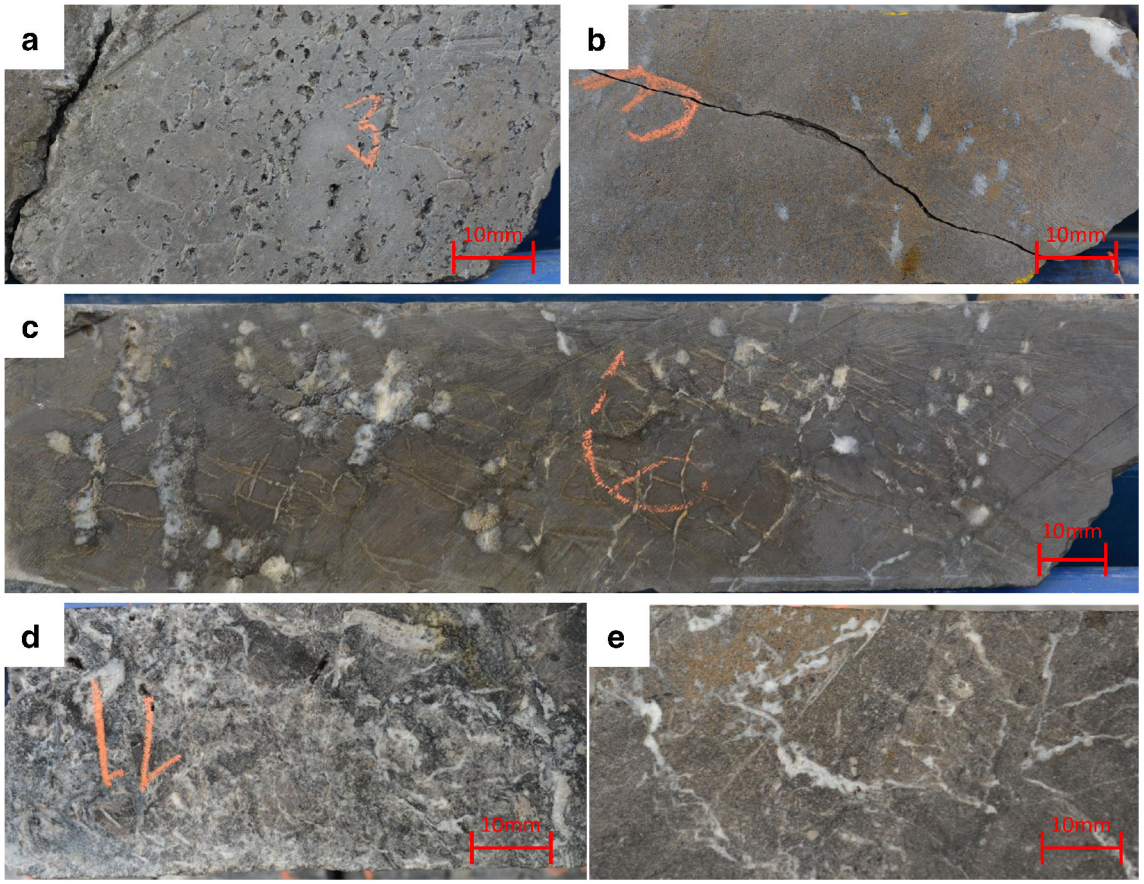

Fig. 5 Drill core samples showing representative rock textures. **a** SH-210-107.70: barren porous dolostone with abundant large vugs. **b** SH-56-287.60: porous dolostone with vugs filled by dark-brown sphalerite and white sparry dolomite. **c** SH-43-173.30: dolomitic mudstone with white calcite pseudomorph after halite. **d** SH-43-540.30: barren evaporite breccia showing chaotic texture composed of dark and white dolomite. **e** SH-43-571.10: evaporite breccia with dark-brown sphalerite filling voids

Chambará II and Chambará III members. These are highly variable in thickness and lateral continuity. They occur more commonly in the Chambará III member that hosts the largest sulfide orebody (Resurgidora) than in the Chambará II member. The textural relationships between Zn–Pb mineralization and replaced evaporite horizons at Shalipayco resemble those at the Florida Canyon MVT deposit north of Shalipayco in the Pucará Basin (de Oliveira et al. 2019b) and in several other MVT deposits worldwide (Charef and Sheppard 1987; Bouabdellah et al. 2014; Bouabdellah et al. 2015; Bouhlel et al. 2016; Leach et al. 2017).

Stratabound Zn–Pb orebodies

The Zn–Pb mineralized zones are composed predominantly of pale yellow sphalerite, dark-brown sphalerite, pyrite, galena, and marcasite (Fig. 6a–h). The Resurgidora level is the largest known orebody. It crops out along most of its lateral extent eroding to a brown colored sulfide-rich detritus. The orebody has an average thickness of 4 m, though it reaches 11 m locally, and extends 4 km along strike. The ores are hosted by Chambará III dolostones and, to a lesser extent, by partially dolomitized mudstones, wackestones, and boundstones. The main ore is composed of coarse zoned sphalerite that is either dark-brown or pale yellow associated with coarse sparry dolomite or with evaporite breccia matrix. In cases where Zn–Pb sulfide minerals have replaced evaporite facies, the dark-brown sphalerite is associated with sparry dolomite interstitial to euhedral barite crystals and, in some cases, the dark-brown sphalerite replaces barite (Fig. 6a, b). Sparry dolomite can occur with pyrite and calcite without sphalerite (Fig. 6c), or with chalcedony (Fig. 6d). In boundstones and mudstones, the sulfides occur as fracture filling within sparry calcite and dolomite (Fig. 6e). Disseminated fine-grained sphalerite occurs as evaporite breccia matrix with galena and interstitial pyrite (Fig. 6f). Bitumen occurrence is widespread in pores and gaps in evaporite breccias commonly associated with sphalerite (Fig. 6g, h) and is more abundant in the fetid dolostone of Chambará III and in the porous dolostone of Chambará II members.

The Intermedios orebody has an average thickness of 8 m, locally reaching 25 m, and extends at least 2 km along strike. The ore sulfides are hosted by the Chambará II member mostly in porous dolostones and to a lesser extent in mudstones and

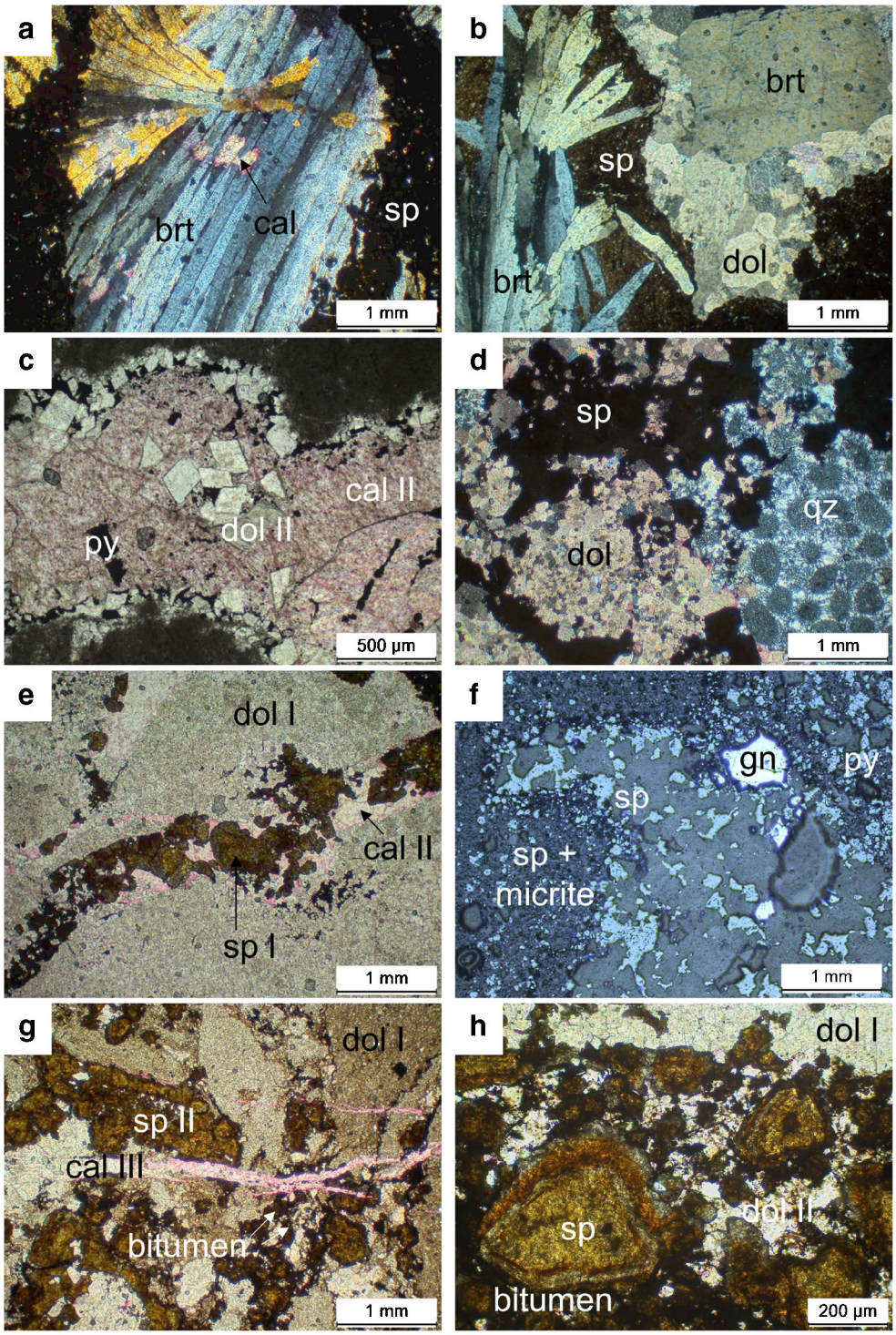

Fig. 6 Photomicrographs. **a** SH-43-196.50: barite within sphalerite with the late replacement by medium-coarse calcite (cal II). **b** SH-43-196.50: barite associated with sparry white dolomite (dol II) filling open space. **c** SH-43-210.30: fracture filled with dolomite and calcite (alizarin red-stained) with pyrite in the vein center. **d** SH-210-253.10: dolostone with sphalerite (sp I) and late chalcedony. **e** SH-120-182.70: dolostone with fractures filled by sphalerite and calcite (alizarin red-stained). **f** SH-231-140.00: disseminated thin sphalerite as breccia matrix with galena and interstitial pyrite. **g** SH-56-284.60: fragments of dolomite (dol I), sphalerite, and bitumen cut by late calcite (cal III) (alizarin red-stained). **h** SH-56-283.40: coarse sphalerite showing concentric color zoning with associated bitumen in dolomitic matrix. brt = barite, cal = calcite, dol = dolomite, gn = galena, py = pyrite, sp. = sphalerite

wackestones. Sphalerite is the most abundant mineral occurring as medium (~ 0.2 mm) crystals within breccia matrix with dolomite intraclasts, disseminations near sparry carbonate bands, and as zoned colloform masses that suggest mineral deposition was locally rapid. In dolostones, medium (< 0.5 mm) euhedral zoned sphalerite crystals are present, along with fine pyrite disseminations and millimeter-thick fracture linings, locally associated with hydrothermal dolomite and chalcedony. Generally, pale yellow sphalerite lines the walls of the fractures, with dark-brown sphalerite toward fracture centers indicating that the dark-brown was the first phase to precipitate. Sulfides locally form fracture-controlled networks or occur as massive concentrations of the two sphalerite generations, pyrite, and galena in breccias (Fig. 6f). In the massive

concentrations, the sphalerite crystals are coarse, euhedral, and locally zoned. In some cases, the sphalerite is fractured, suggesting tectonic activity after precipitation in dissolution cavities along with sparry calcite (Fig. 6e). Sparry calcite veins cut sulfide mineralization.

Additional occurrences of Zn–Pb sulfides are present in porous dolostone horizons within the Chambará I member, but these occurrences are of restricted lateral extent and thickness and are generally low grade. These include the Virgencite, San Luis, and Pucará levels (Tuanama 2016). Also, sphalerite, galena, pyrite, chalcopyrite, and iron oxides have been identified in surface exposures that trend N170 and dip 75E. This trend, which is referred to as the Eddy vein (Fig. 2), does not appear to extend into the subsurface.

3D geological modeling

Three-dimensional geological modeling confirms the lateral extent of the four members of the Chambará Formation. The model depictions shown in Fig. 4 show that the Resurgidora and Intermedios orebodies are restricted to the Chambará III and Chambará II members, respectively. For this initial model of the Shalipayco geology, the focus was on lithologic rather than structural constraints. Although the deposit lies within a fold and thrust belt, the sole structural feature included in the model is tilting of all strata with a dip direction of 225°/30°SW, which also dictates the direction of the Zn–Pb mineralized horizons (Fig. 4). Later NW-trending faults were not considered due to the work scale issues. The displacement of these faults is apparently only a few meters, and the model reproduces geological units at least on the decametric scale; also, the current drilling spacing is very large. Nevertheless, future drilling would enable the 3D model with disposition of regional-scale faults to be updated.

Paragenetic sequence

The Shalipayco mineral paragenesis can be divided into four stages: (1) early diagenetic stage, (2) burial diagenetic stage, including pre-Zn–Pb dolomitization, (3) Zn–Pb ore formation (main ore stage), and (4) post-ore stage (Fig. 7). Primary micritic calcite, coarser calcite particles (cal I), and other allochems, such as oolites and oncoids, underwent varying degrees of dolomitization during burial diagenesis. Evaporite minerals, probably including gypsum and/or anhydrite and halite, were entirely dissolved and replaced by sparry dolomite (dol I) or secondary calcite. Dolomitization was extensive in the Zn–Pb mineralized Chambará II and III members, to the extent that original sedimentary textures were completely obliterated, and the rock was entirely replaced by sparry dolomite (dol I). Pale dolomite and boundstone of the upper Chambará III member experienced less intense dolomitization so that oolites, oncoids, and micritic matrix are locally well preserved.

Zn–Pb ore formation began with the precipitation of finely crystalline pyrite between sparry dolomite crystals. Precipitation of pale yellow and dark-brown sphalerite (possibly in a continuum rather than in distinct events), galena, and new forms of pyrite followed, locally with associated or slightly later white sparry dolomite (dol II) (Fig. 6h). Marcasite is locally associated with pyrite and sphalerite in later stages. This second generation of dolomite (dol II) fills open fractures and is present in breccia matrices. In weakly dolomitized or undolomitized rocks with preserved micritic textures, barite fills fractures that predated deposition of fine- to medium-grained zoned sphalerite (Fig. 6a). Barite also occurs as larger crystals in disordered arrangement and as euhedral acicular crystals (Fig. 6b). Chalcedony precipitated late in the Zn–Pb mineralization stage, locally cutting ore sulfides and filling cavities that originally contained evaporite nodules. Finally, post-mineralization, fine- to medium-grained calcite (cal III) occurs as millimeter-wide veins (Fig. 6g), open-space fillings, and replacements.

Fluid inclusions

Fluid inclusions are single phase (liquid) for early replacement dolomite (dol I) and two phase (liquid + vapor) for late sparry dolomite (dol II) and sphalerite. The inclusions are less than 8 μm in diameter, which are too small for reliable microthermometry. However, an upper-temperature limit can be placed on the early replacement dolomite stage by the fact that entrapment temperatures for the single-phase inclusions are unlikely to have exceeded 40–50 °C (Goldstein and Reynolds 1994).

Whole-rock geochemistry

Analyses of 21 elements in whole-rock drill core powders at intervals of approximately 1 m were provided by Nexa Resources. Elements with concentrations below the detection limit in many samples (Be, Bi, and W) were excluded from the database. For the purpose of calculating range and median, the results were separated into four groups: unmineralized carbonate host rock ($n = 19{,}023$), Intermedios orebody ($n = 858$), Resurgidora orebody ($n = 460$), and Eddy vein occurrence ($n = 197$) (Table 1). The median concentrations of Co, Cr, Mo, Ni, Sr, and V are similar in the four groups. The maximum concentrations of Ba, Mn, and Ti are higher in the carbonate host-rocks (9120, 14,750, and 28,100 ppm, respectively) than the Intermedios orebody (440, 3690, and 9900 ppm, respectively), Resurgidora orebody (3820, 10,200, and 1300 ppm, respectively), and Eddy vein (330, 3990, and 8700 ppm, respectively). Maximum concentrations of In tend to be higher in the sulfide-rich mineralized samples (21 ppm

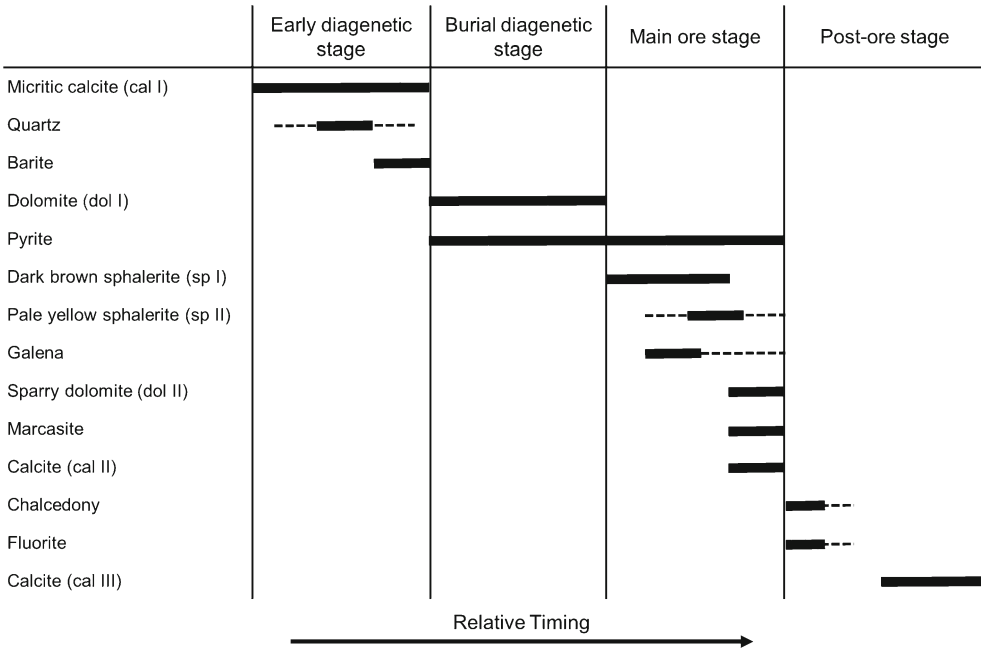

Fig. 7 The paragenetic sequence of the Shalipayco deposit. Dashed lines reflect decreasing relative abundance of minerals

for Intermedios and 12 ppm for Eddy vein) than in unmineralized host rock (9 ppm), although the Resurgidora orebody is lower (3 ppm). Median concentrations of Ag, As, Cd, Cu, Hg, and Sb are also higher in sulfide ores (Intermedios, Resurgidora, and Eddy vein) than in the unmineralized carbonate host rock. These same six elements are much higher in the Eddy vein occurrence than the Intermedios and Resurgidora sulfide bodies (Fig. 8). The

Table 1 Selected trace element ranges and median (ppm) (in italics) of drill core whole-rock samples in the carbonate host rock, the Intermedios orebody, the Resurgidora orebody, and the Eddy vein occurrence within the Shalipayco deposit

	Non-mineralized carbonate host rock $n = 19{,}023$	Intermedios stratabound orebody $n = 858$	Resurgidora stratabound orebody $n = 460$	Eddy vein occurrence $n = 197$
Ag	0.005–272 (*1.3*)	0.25–217 (*17*)	0.19–174 (*12*)	2.8–916 (*124*)
As	1–5860 (*49*)	15–4220 (*138*)	10–2500 (*132*)	2.5–7040 (*261*)
Ba	1–9120 (*5*)	5–440 (*5*)	5–3820 (*60*)	5–330 (*5*)
Be	0.02–3.9 (*0.3*)	0.02–0.8 (*0.3*)	0.18–0.9 (*0.3*)	0.02–1.3 (*0.3*)
Bi	0.005–12 (*1*)	0.005–6 (*1*)	0.005–4 (*1*)	0.005–20 (*1*)
Cd	0.01–971 (*1*)	0.21–1310 (*81*)	0.18–791 (*50*)	0.25–3140 (*452*)
Co	0.1–604 (*1*)	0.4–41 (*2*)	0.5–16 (*1*)	0.1–850 (*2*)
Cr	0.5–625 (*2*)	0.5–198 (*1*)	0.5–13 (*1*)	0.5–156 (*2*)
Cu	0.1–2300 (*2*)	0.5–634 (*18*)	0.5–154 (*2*)	0.5–21,500 (*26*)
Hg	0.01–359 (*0.3*)	0.05–271 (*13*)	0.01–171 (*8*)	0.01–317 (*42*)
In	0.005–9 (*0.01*)	0.005–21 (*0.12*)	0.005–3 (*0.01*)	0.005–12 (*0.01*)
Mn	25–14,750 (*1610*)	431–3690 (*1500*)	935–10,200 (*3705*)	6–3990 (*916*)
Mo	0.05–49 (*1*)	0.08–196 (*0.5*)	0.19–18 (*3*)	0.09–17 (*1*)
Ni	0.1–512 (*2*)	0.1–170 (*1*)	0.1–15 (*1*)	0.1–1780 (*1*)
Pb	1–266,000 (*51*)	10–94,300 (*291*)	11–122,000 (*1723*)	15–479,100 (*889*)
Sb	0.02–2010 (*5*)	2.5–514 (*29*)	2.5–578 (*20*)	2.5–7110 (*93*)
Sr	3–8210 (*93*)	25–2980 (*57*)	47–2780 (*150*)	4–4310 (*56*)
Ti	25–28,100 (*100*)	25–9900 (*50*)	50–1300 (*100*)	25–8700 (*50*)
V	0.5–324 (*5*)	0.5–126 (*1*)	0.5–46 (*7*)	0.5–176 (*1*)
W	0.05–220 (*5*)	0.05–80 (*5*)	0.1–70 (*5*)	0.05–70 (*10*)
Zn	1–384,300 (*165*)	72–388,400 (*28,800*)	120–260,000 (*21,750*)	5–520,700 (*135,500*)

The median values are given in parentheses; n = number of samples

median concentrations of Ag, As, Cd, Cu, Hg, and Sb are 124, 261, 452, 26, 42, and 93 ppm in the Eddy vein occurrence, whereas in the Intermedios and Resurgidora orebodies, they are 17, 138, 81, 18, 13, and 29 ppm, and 12, 132, 50, 2, 8, and 20 ppm, respectively (Table 1).

The distribution of elements relative to major faults was examined in plain view (Fig. 8). In the Shalipayco deposit, two patterns of faults are recognized. Older structures are NW-directed thrust faults (e.g., Eddy vein) and younger faults are N-striking (Figs. 2 and 8). Concentrations of Ag, As, Cd, Cu, Hg, and Sb are higher near the Eddy vein structure (345°/80°NE) than in the Intermedios and Resurgidora orebodies with a general dip direction of 225°/30°SW (Figs. 4 and 8).

Carbon, oxygen, and strontium isotopes

Samples for C and O isotopic analyses were selected based on petrography and representativeness modes of the different carbonate generations as well as their relationship to sulfides. The results are presented in Table 2 and Fig. 9, together with data from Moritz et al. (1996). The samples from Moritz et al. (1996) were probably obtained from outcrops and, in the original work, the local spatial position is not specified. Overall, the results of Shalipayco samples exhibit a positive correlation between $\delta^{13}C$ and $\delta^{18}O$ (Fig. 9). Carbonate samples become isotopically lighter through the paragenetic sequence such that the later calcite (cal II and III) has negative $\delta^{13}C$ and significantly lower $\delta^{18}O$.

The limestone (cal I) samples have $\delta^{13}C$ values between 1.8 and 1.9‰ and $\delta^{18}O$ values between 27.8 and 30.8‰. These rocks are interpreted to be the least altered and present the highest $\delta^{18}O$ values (Fig. 9). The limestone (cal I) samples plot entirely within the field of Triassic marine limestone (Veizer et al. 1999). These high $\delta^{18}O$ values are consistent with evaporitic conditions and high salinities implied by the occurrence of evaporite pseudomorphs in these rocks. Limestone (I) samples from Moritz et al. (1996) are probably unmineralized but not from evaporitic horizons, and therefore, they have slightly lower $\delta^{18}O$ values compared to the limestone (cal I) samples from this study. Some samples of sparry dolomite (dol II) and dolostone (dol I) that interacted with fluids associated with the ore-stage sulfides plot partially in the Triassic limestone field (Veizer et al. 1999). The dolomite samples from Moritz et al. (1996) identified as repl. dol (I) and sparry dol. II show $\delta^{18}O$ values between 24.4 and 26.2‰ and $\delta^{13}C$ values between 1.1 and 2.1‰, close to those obtained in this study. This set of samples has $\delta^{13}C$ values between − 0.1 and 2.1‰ and of $\delta^{18}O$ values between 17.5 and 26.2‰. The similarity between the host dolostone (dol I) and the ore-associated sparry dolomite (dol II) suggests that the isotopic composition of the dolomitizing fluid was controlled by exchange with the host rocks. The calcite samples from late veins (cal II) related to sulfide ore (Fig. 6c, e), as well as the coarse calcite (II) samples from Moritz et al. (1996), show the lowest values for both $\delta^{13}C$ (− 2.9 to − 0.5‰) and $\delta^{18}O$ (11.0 to 16.1‰). The lighter C and O isotopic signatures may reflect the involvement of meteoric water during dedolomitization. The late calcite (cal III) sample shows a $\delta^{18}O$ value of 13.3‰ within the range of the other calcites (cal II), but also the lowest $\delta^{13}C$ value (− 5.1‰).

The general isotopic similarity between burial diagenetic dolomite (dol I) and later void-filling sparry dolomite related to ore-stage sulfides (dol II) is a feature that was also observed at the Florida Canyon deposit (Fig. 9) farther north in the Pucará Basin (de Oliveira et al. 2019b). At Shalipayco, at least, in locations where the two dolomite types were collected in close physical proximity, later sparry dol II was slightly lighter in C and O than earlier dol I (sparry dolomite in sample SH-43-571.10 has $\delta^{18}O = 17.5‰$ and $\delta^{13}C = -0.1‰$ whereas replacement dolostone in sample SH-43-519.80 has $\delta^{18}O = 24.5‰$ and $\delta^{13}C = 0.2‰$) (Table 2).

Strontium isotope results (Table 3, Fig. 10) also reveal distinct ranges for the major carbonate stages, much like the strontium isotope results for carbonate stages in the Florida Canyon deposit (de Oliveira et al. 2019b). The data of Moritz et al. (1996) differentiate limestone (cal I), which has values within the characteristic range for Triassic seawater (Koepnick et al. 1990; Korte et al. 2003), burial diagenetic replacement dolomite (dol I), which has values extending to slightly more radiogenic compositions, and late coarse calcite (cal II), which has the most radiogenic values. Three samples of Mitu group alkali basalt show compositions ($^{87}Sr/^{86}Sr$ values of 0.709654 to 0.719669) that are more radiogenic than any of the Shalipayco carbonates (0.707650 to 0.708980).

Sulfur isotopes

Sulfur isotope compositions were determined for sphalerite (two generations), galena, pyrite, and barite from the Resurgidora and Intermedios orebodies (Table 4, Fig. 11). The $\delta^{34}S$ values of each of these minerals from the Resurgidora and Intermedios orebodies overlap within error, and they do not vary consistently with depth or paragenetic position. The two barite samples, which predate Zn–Pb sulfides in the paragenesis, have $\delta^{34}S$ values of 13.7 and 17.3‰, overlapping the range of values that characterizes the Middle Triassic to Jurassic seawater sulfate (15 to 17‰, Claypool et al. 1980; Kampschulte and Strauss 2004). The $\delta^{34}S$ values for dark-brown sphalerite (sp I) range from − 19.1 to − 16.8‰ and for pale yellow sphalerite (sp II) from − 17.9 to − 15.3‰, whereas the galena values range from − 23.0 to − 10.4‰. Pyrite $\delta^{34}S$ values show a wider range, from − 23.3 to − 6.2‰. Sphalerite-galena mineral pairs in samples SH-120-109.80 and SH-231-140.90 (Table 4) give isotopic equilibration temperatures of 139 and 159 °C, respectively (Ohmoto and Rye 1979), similar to fluid inclusion homogenization

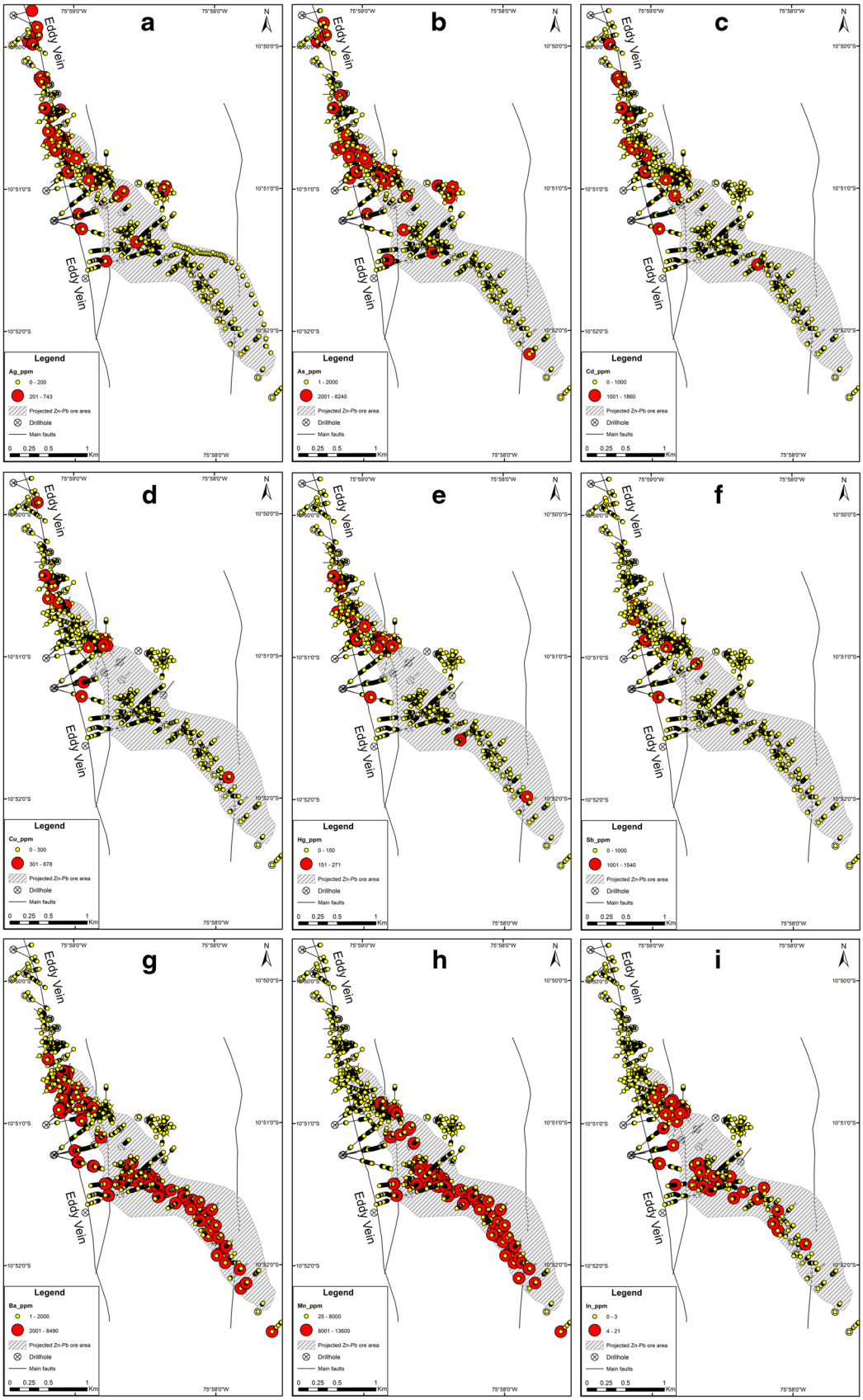

Fig. 8 Plan view of trace and minor elements in drill core samples of the Shalipayco deposit. **a** Silver. **b** Arsenic. **c** Cadmium. **d** Copper. **e** Mercury. **f** Antimony. **g** Barium. **h** Manganese. **i** Indium

temperatures of ore-related sparry dolomite (dol II) (115 to 162 °C, Moritz et al. 1996).

Discussion

Lithostratigraphic and structural constraints

The main orebodies in the Shalipayco deposit are hosted by the most porous and permeable units of the Chambará carbonate sequence, the Chambará II and Chambará III members. The higher porosity and permeability partly reflect an abundance of former evaporite minerals in these units. Former evaporite mineral occurrences were the most laterally extensive in the Chambará III member, which may explain the greater lateral extent and higher metal contents of the Resurgidora orebody compared to the Intermedios orebody. The enhanced permeability probably resulted from volume reduction associated with evaporite mineral replacement reactions and also from brecciation caused by calcium sulfate dissolution. These dolomitization processes may have generated H_2S gas that would furnish reduced sulfur for later Zn–Pb sulfide precipitation (Anderson and Garven 1987; Worden and Smalley 1996). Alternatively, given the abundance of bitumen in the Chambará III member, the H_2S generated during dolomitization may have been associated with a former oil reservoir. The Chambará I and Chambará IV members, which consist predominantly of mudstones and packstones, also may have influenced ore formation by serving as aquitards that favored H_2S retention in the more porous intervening strata and restricted flow of metalliferous fluids within the H_2S-rich zones. Steeply dipping faults would have been essential in allowing metalliferous fluids from deeper in the stratigraphic section to penetrate the Chambará I aquitard and access the more permeable, H_2S-bearing Chambará II and Chambará III members.

The Shalipayco deposit fault setting is characterized by regional primary northwest thrust faults and local secondary north-northeast, north, and north-northwest steeply dipping structures that may have controlled different styles of mineralization. The regional thrust faults may have had some strike-slip movement during acquiescence periods in the orogenesis evolution. Therefore, assuming a Riedel model (Petit 1987), the north-northeast, north, and north-northwest secondary structures would be a product of these movements. However, the secondary structures differ in relation to the metalliferous sulfide occurrences where N faults are related to Zn–Pb orebodies whereas NNW faults are related to Cu–Pb–Zn Eddy vein structure. The north-trending faults that intersect the stratabound Zn–Pb orebodies (Fig. 8) are considered to have been the main conduits for ascending metalliferous brines (de Oliveira et al. 2020). Alternatively, the north-northwest Eddy vein structure that contains shallow copper sulfides is expressed as abundant veins on the surface that become rarer to absent at 50 m depth, suggesting an epithermal setting. The concentration of the Ag, As, Cd, Cu, Hg, and Sb elements around the Eddy vein (Fig. 8) is consistent with this hypothesis. The carbonate-hosted replacement ores in Cerro de Pasco are also controlled along northwest faults (325°) in addition to faults of 190°, 240°, and 270° directions (Baumgartner et al. 2008).

Table 2 Carbon and oxygen isotope composition of carbonates of the Shalipayco deposit

Sample	Orebody/ member	Description (paragenetic stage)	$\delta^{18}O_{VSMOW}$(‰)	$\delta^{13}C_{VPDB}$(‰)
SH-60-171.50-R	Intermedios	Limestone (cal I)	30.8	1.9
SH-60-174.40-R	Intermedios	Limestone (cal I)	30.4	1.9
SH-60-170.40	Resurgidora	Limestone (cal I)	30.7	1.7
SH-70-217.60	Resurgidora	Limestone (cal I)	27.8	1.8
SH-43-519.80	Chambará I	Dolostone (dol I)	24.5	0.2
SH-56-298.20-R	Intermedios	Dolostone (dol I)	25.9	1.7
SH-43-359.30	Intermedios	Dolostone (dol I)	20.9	1.5
SH-70-220.00	Resurgidora	Sparry dolomite (dol II)	25.3	1.0
SH-43-571.10	Chambará I	Sparry dolomite (dol II)	17.5	− 0.1
SH-120-173.00	Intermedios	Calcite (cal II)	14.8	− 0.8
SH-120-171.00	Intermedios	Calcite (cal II)	13.4	− 1.3
SH-56-298.20-C	Intermedios	Calcite (cal II)	11.0	− 1.0
SH-180-189.70	Resurgidora	Calcite (cal II)	16.1	− 0.5
SH-120-109.80	Resurgidora	Calcite (cal II)	14.7	− 1.4
SH-231-134.60	Intermedios	Calcite vein (cal III)	13.3	− 5.1

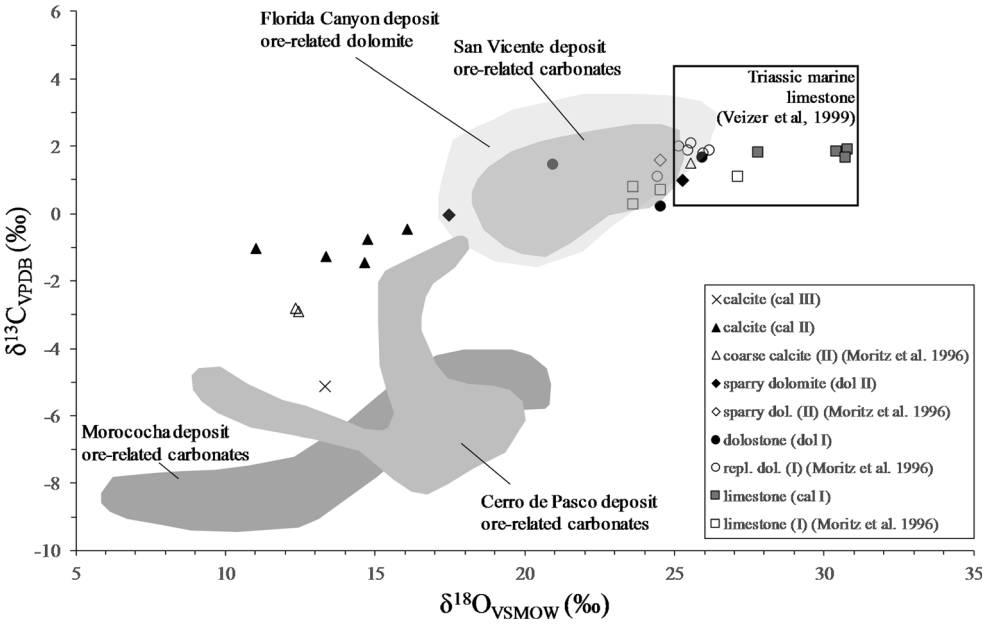

Fig. 9 Plot of $\delta^{13}C$ vs $\delta^{18}O$ showing measured values for carbonate samples from the Shalipayco deposit (Table 2 and Moritz et al. 1996) and values for ore-related carbonates at the Florida Canyon (de Oliveira et al. 2019b), San Vicente (Spangenberg et al. 1996), Morococha (Catchpole et al. 2015a) and Cerro de Pasco (Baumgartner et al. 2008) deposits are shown for comparison

Origin of hydrothermal fluids

Classification of the Shalipayco deposit as MVT implies that the ores precipitated from basin brines at temperatures of 90–150 °C, the range of homogenization temperatures typically observed in studies of MVT fluid inclusions (Leach et al. 2005). On the other hand, the classification of Shalipayco as a carbonate-replacement deposit would imply that the ores precipitated from a dominantly magmatic fluid at temperatures of 200–500 °C, the range of homogenization typically observed in studies of carbonate-replacement type ores (Megaw et al. 1988).

Measured $\delta^{18}O$ values of Shalipayco dol II range from 17.5 to 25.3‰ (Table 2). Calculated $\delta^{18}O$ values of fluids in equilibrium with sparry dol II, based on temperatures of 200–500 °C and fractionation factors from Zheng (1993), are about 16 ± 4‰, much higher than the normal range for magmatic fluids (5.5–10‰, Taylor, 1974). The dol II compositions are thus inconsistent with a carbonate-replacement origin for the Shalipayco ores. Further support for an MVT model can be found in fluid inclusion petrography. The single-phase fluid inclusions in replacement dolomite (dol 1) are consistent with entrapment during diagenesis at 40–50 °C, whereas 2-phase inclusions in sparry dolomite studied by Moritz et al. (1996) imply entrapment temperatures of 115 to 162 °C and brine-like salinities of 9.5–26 wt.% NaCl equivalent. These observations are consistent with a MVT model for Shalipayco, but contrast with the Morococha epithermal occurrence, which shows evidence of significantly lower salinities (2–5 wt.% NaCl equivalent) and significantly higher temperatures (220–260 °C, Catchpole et al. 2011).

The oxygen isotope composition of the Shalipayco carbonates is similar to that for the San Vicente (Fontboté and Gorzawski 1990; Spangenberg et al. 1999) and Florida Canyon (de Oliveira et al. 2019b) MVT deposits, but contrasts with the oxygen isotope compositions for the Cerro de Pasco (Baumgartner et al. 2008) and Morococha (Catchpole et al. 2015a) magmatic-related deposits. Cerro de Pasco ore-related carbonates have $\delta^{13}C$ values (− 8.1 to 1.0‰) and $\delta^{18}O$ values (9.5 to 19.5‰), which differ from the values of the unaltered Pucará host rocks, 1.4 to 2.7‰ for $\delta^{13}C$ values, and 19.2 to 25.3‰ for $\delta^{18}O$ values (Baumgartner et al. 2008). The lower $\delta^{13}C$ values at Cerro de Pasco are consistent with a magmatic origin for the carbon (Baumgartner et al. 2008). Similarly, low $\delta^{13}C$ values characterize ore-related carbonates from the Morococha polymetallic vein and replacement deposits (Catchpole et al. 2015a). The low $\delta^{13}C$ values could reflect fluid interaction with organic-rich horizons in the Pucará group country rocks. However, sulfides in the Morococha district yield $\delta^{34}S$ values near zero permil (Catchpole et al. 2015a), which is more consistent with a magmatic fluid

Table 3 Strontium isotope compositions for the Chambará Formation limestone and the Mitu group alkali basalt in the vicinity of the Shalipayco deposit

Sample	Mineral/Rock	$^{87}Sr/^{86}Sr$	2 s
SH-56-298.20-N	Chambará Fm. limestone	0.708254	0.000020
SH-70-217.60-N	Chambará Fm. limestone	0.708021	0.000038
SH-60-170.40-N	Chambará Fm. limestone	0.708208	0.000015
SH-43-683.90-M	Mitu Gp. alkali basalt	0.719669	0.000019
SH-43-684.70-M	Mitu Gp. alkali basalt	0.709996	0.000017
SH-43-685.90-M	Mitu Gp. alkali basalt	0.709654	0.000017

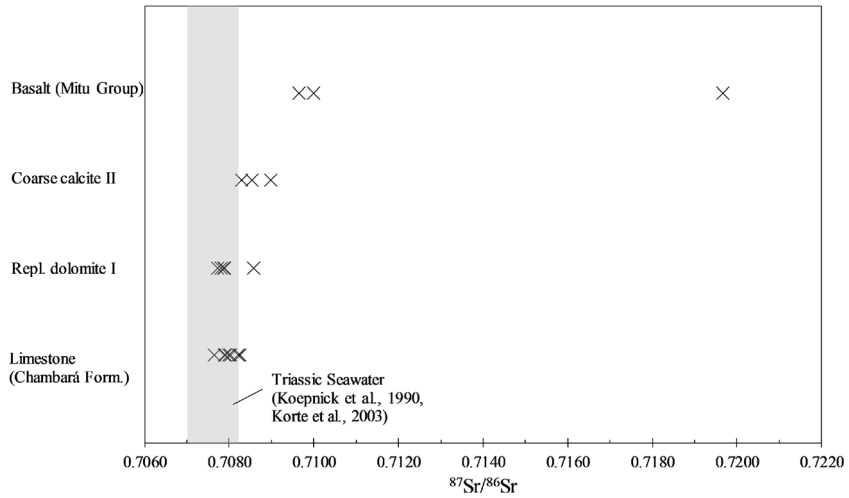

Fig. 10 Sr isotope compositions of the different stages of carbonates from the Chambará Formation of Shalipayco deposit and basalts from the Mitu group (data from Table 3). Data from limestone, replacement dolomite, and coarse calcite from Moritz et al. (1996). The limestone sample data from this study ($n = 3$) and from Moritz et al. (1996) ($n = 4$) are plotted together and overlap

origin than a basinal fluid origin (Hoefs 1980). The decrease in carbonate $\delta^{13}C$ values through the Shalipayco paragenesis probably reflects increasing importance of organic matter oxidation (Carothers and Kharaka 1980).

The Chambará Formation limestones and diagenetic replacement dolomite (dol I) exhibit similar $^{87}Sr/^{86}Sr$ ranges, 0.707650–0.708254 and 0.70773–0.70857, respectively, that correspond closely to the range in Norian seawater (0.7075–0.7082, Koepnick et al. 1990; Korte et al. 2003). The correspondence suggests that the dolomitizing fluids had circulated through, and acquired solutes from, calcareous strata within the Pucará group. The $^{87}Sr/^{86}Sr$ values of ore-related coarse calcite (cal II, 0.70830–0.70898) are more radiogenic, which implies that the ore-forming fluid transported strontium, and perhaps other metals, from other sources, perhaps the Mitu group alkali basalt (0.709654–0.719669) or strata with higher Rb/Sr ratios (Moritz et al. 1996).

Source of sulfur and mechanisms of sulfide precipitation

Textural observations suggest that the reductive dissolution of gypsum and anhydrite in evaporite horizons of the Pucará group was likely a source of at least some of the sulfur required to form the Shalipayco ores. If this assumption is correct, H_2S could have been produced by mechanisms similar to those that produce high concentrations of H_2S in natural gas reservoirs. At temperatures sufficient to sustain thermochemical sulfate reduction—the lower temperature threshold

Table 4 Sulfur isotope compositions of sphalerite, galena, pyrite, and barite from the Shalipayco deposit

Sample	Orebody	Mineral	$\delta^{34}S_{VCDT}$(‰)
SH-56-298.20-O	Intermedios	Barite	17.3
SH-70-220.00-O	Resurgidora	Barite	13.7
SH-120-109.80-G	Resurgidora	Galena	− 23.0
SH-231-140.90-G	Intermedios	Galena	− 22.2
SH-43-221.70-G	Resurgidora	Galena	− 10.4
SH-210-219.70-H	Intermedios	Pyrite	− 21.3
SH-43-221.70-H	Resurgidora	Pyrite	− 6.2
SH-43-248.60-H	Intermedios	Pyrite	− 23.3
SH-120-109.80-E	Resurgidora	Dark-brown sphalerite (sp I)	− 19.1
SH-120-113.80-E	Resurgidora	Dark-brown sphalerite (sp I)	− 18.0
SH-120-175.60-E	Intermedios	Dark-brown sphalerite (sp I)	− 16.8
SH-56-287.60-E	Intermedios	Dark-brown sphalerite (sp I)	− 17.0
SH-120-175.60-F	Intermedios	Pale yellow sphalerite (sp II)	− 15.3
SH-231-140.90-F	Intermedios	Pale yellow sphalerite (sp II)	− 17.9
SH-231-44.30-F	Resurgidora	Pale yellow sphalerite (sp II)	− 16.1
SH-60-171.50-F	Resurgidora	Pale yellow sphalerite (sp II)	− 16.4

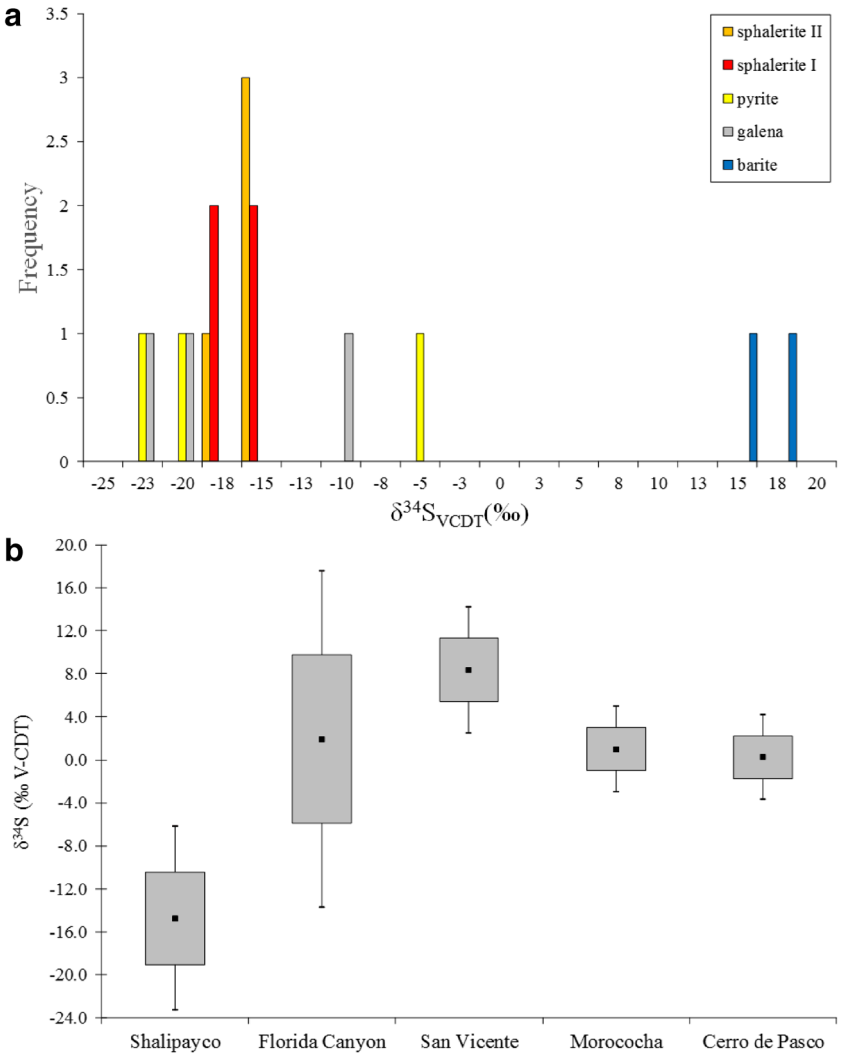

Fig. 11 **a** Histogram of $\delta^{34}S$ values for sphalerite, galena, pyrite, and barite. **b** Boxplot of $\delta^{34}S$ values for sulfides from Shalipayco (Table 4), Florida Canyon (de Oliveira et al. 2019b), San Vicente (Fontboté and Gorzawski 1990; Spangenberg et al. 1999; Schütfort 2001), Morococha (Kouzmanov et al. 2008), and Cerro de Pasco (Baumgartner et al. 2008) deposits

depends on kinetic factors but may be as low as 100 °C (Machel 2001), sulfate minerals can be reduced by reaction with methane or other hydrocarbons, or by reaction with H_2S that had been produced by bacterial sulfate reduction during diagenesis. The fact that the Shalipayco ore sulfides have substantially lower $\delta^{34}S$ (− 23.3 to − 6.2‰) than Triassic-Jurassic marine sulfate values (~ + 12 to + 18‰, Claypool et al. 1980) that are assumed to be equivalent to replaced gypsum and anhydrite strongly suggests that the overall mechanism involved reactions such as (Worden and Smalley 1996):

$$CaSO4 + CO2 + 3H2S => CaCO3 + 4S + 3H2O, \text{ and}$$
$$4S + CH4 + 2H2O => CO2 + 4H2S.$$

In this reaction, three quarters of the product S^{2-} is from H_2S that originated by bacterial sulfate reduction and is isotopically light. This would impart a low $\delta^{34}S$ value to Zn and Pb sulfide minerals. Interestingly, the Zn–Pb sulfides in the San Vicente and Florida Canyon MVT deposits are isotopically heavier than the Shalipayco sulfides, + 2.5 to + 14.2‰ (Fontboté and Gorzawski 1990; Spangenberg et al. 1999; Schütfort 2001) and − 13.7 to + 17.6‰ (Basuki et al. 2008), respectively. The values for San Vicente and Florida Canyon sulfide minerals extend to the composition of Triassic-Jurassic marine sulfate, which was presumably the composition of the evaporitic sulfate minerals at these localities. The sulfur isotope differences between the three deposits can be explained by invoking thermochemical sulfate reduction pathways that differ in detail, the pathways operative at San Vicente and Florida Canyon reliant predominantly on hydrocarbons for sulfate reduction and the pathways operative at Shalipayco reliant to a greater extent on preexisting H_2S of bacterial origin.

The sulfur isotope compositions of sulfides at the Cerro de Pasco (− 3.7 to + 4.2‰, Baumgartner et al. 2008) and Morococha (−3.0 to +5.0‰, Kouzmanov et al. 2008) epithermal deposits are compatible with a magmatic sulfur source (Ohmoto 1986) in that they span restricted ranges with

an average 0 ± 4‰ (Beaty et al. 1990; Thompson and Beaty 1990). The Shalipayco sulfides yield negative values (− 6.2 to − 23.3‰), at least 10 to 20‰ lower, reinforcing the interpretation that the ore sulfur was derived from a nonmagmatic source.

Concluding remarks

1. The observations of various features in the Shalipayco deposit are known to be characteristic of MVT deposits worldwide (Leach and Sangster 1993; Leach et al. 2005): (1) the Chambará Formation host rocks are platform carbonates with evaporite sequences within the Andean orogenic foreland fold-and-thrust belt; (2) the sulfide mineralization occurs in dolostones and is clearly epigenetic and stratabound in morphology; (3) the ore mineralogy is simple with sphalerite, galena, pyrite, quartz, dolomite, calcite, barite, and fluorite; and (4) sulfur data show isotopic evidence for crustal sources.
2. The 3D geological modeling confirms the new local subdivision of the Chambará Formation into laterally continuous four members in the vicinity of the Shalipayco deposit. The main Zn–Pb sulfide orebodies Resurgidora and Intermedios in the 3D model are restricted to the Chambará III and Chambará II members, respectively, confirming a lithological constraint for the sulfide ore.
3. The results of sulfur, carbon, and oxygen isotope analyses, together with the temperature constraints from fluid inclusion petrography, and sulfur isotope geothermometry (< 160 °C) at the Shalipayco deposit are consistent with a MVT origin. The location in the same carbonate sequence and geographic region as skarn deposits (Atacocha and Milpo) and epithermal deposits (Cerro de Pasco, Colquijirca, and Morococha) are thought to be coincidental.
4. The Eddy vein occurrence shows a geochemical signature of elevated Ag, As, Cd, Cu, Hg, and Sb, which is similar to that of the Cerro de Pasco epithermal deposits. Therefore, the sulfide occurrences of the Eddy vein and the Zn–Pb MVT orebodies of Resurgidora and Intermedios may be different deposit types that could have been temporally distinct events with distinct structural controls. However, specific studies in the Eddy vein should be made to prove this hypothesis.
5. The Shalipayco deposit is contained in strata that closely resemble the host strata for the Florida Canyon deposit farther north in the Pucará Basin. These strata lie near the base of the Pucará group, and they exhibit evidence for the same ground preparation prior to ore formation that resulted in highly porous dolostone, evaporite breccia, and evaporite pseudomorphs. The ore textures and sulfide forms are also similar, leading to the conclusion that they were formed by similar metalliferous brines and by similar precipitation mechanisms. Undiscovered MVT deposits of the evaporite type could exist elsewhere in the Pucará group.

Acknowledgments The authors would like to thank all field geologists, including Daniel Hinostroza and Nancy Tuanama for discussions during fieldwork, and Pan American Silver and Nexa Resources for the use of data. We wish also to thank Jim Reynolds for discussions about fluid inclusions and Cayce Gulbransen, for assistance during S isotope analysis. We also would like to thank Editor-in-Chief Georges Beaudoin, Associate Editor Karen Kelly, Richard Moscati, Janet Slate, and the anonymous reviewer for their careful reading of our manuscript and their suggestions and comments, which surely improved the quality of the paper. This paper is part of the first author's Ph.D. thesis (Instituto de Geociências, Universidade de São Paulo) part of this work was conducted during a visiting scholar period at Colorado School of Mines, sponsored by the Capes Foundation within the Ministério da Educação, Brazil (process 88881.135448/2016-01), that the authors would like to thank. Any use of trade, firm, or product names is for descriptive purposes only and does not imply endorsement by the US Government.

References

Anderson GM, Garven G (1987) Sulfate-sulfide-carbonate associations in Mississippi Valley-type lead-zinc deposits. Econ Geol 82:482–488

Baby P, Calderón Y, Hurtado C, Louterbach M, Espurt N, Brusset S, Roddaz M, Brichau S, Eude A, Calvès G (2019) The Peruvian sub-andean foreland basin system: structural overview, geochronologic constraints, and unexplored plays In: Zamora G, McClay KR, Ramos VA (eds) Memoir 117: Petroleum Basins and Hydrocarbon Potential of the Andes of Peru and Bolivia. AAPG Special Volumes, pp 87–116

Badoux V, Moritz R, Fontboté L (2001) The Mississippi Valley-type Zn-Pb deposit of San Vicente, Central Peru: an Andean syntectonic deposit. Mineral deposits at the beginning of the 21th Century Proceed Joint 6th Biennial SGA-SEG Mtg, Krakow, Poland:191–195

Basuki NI, Taylor BE, Spooner ETC (2008) Sulfur isotope evidence for thermochemical reduction of dissolved sulfate in Mississippi Valley-type zinc-lead mineralization, Bongara area, northern Peru. Econ Geol 103:783–799

Baumgartner R, Fontboté L, Vennemann T (2008) Mineral zoning and geochemistry of epithermal polymetallic Zn-Pb-Ag-Cu-Bi mineralization at Cerro de Pasco, Peru. Econ Geol 103:493–537

Beaty DW, Landis GP, Thompson TB (1990) Carbonate-hosted sulfide deposits of the Central Colorado Mineral Belt: introduction, general discussion and summary in: Beaty DW, Landis GP. Thompson TB (eds) Economic Geology Monograph 7:1–18

Benavides-Cáceres V (1999) Orogenic evolution of the Peruvian Andes: the Andean cycle. Geology and ore deposits of the Central Andes 7: 61–107

Benavides V (1968) Saline deposits of South America International Conference on Saline Deposits. pp 249-290

Bendezú R, Fontboté L, Cosca M (2003) Relative age of Cordilleran base metal lode and replacement deposits, and high sulfidation Au-(Ag) epithermal mineralization in the Colquijirca mining district, central Peru. Mineral Deposita 38:683–694. https://doi.org/10.1007/s00126-003-0358-z

Bendezú R, Fontboté L (2009) Cordilleran epithermal Cu-Zn-Pb-(Au-Ag) mineralization in the Colquijirca district, central Peru: deposit-scale mineralogical patterns. Econ Geol 104:905–944

Bouabdellah M, Castorina F, Bodnar RJ, Banks D, Jébrak M, Prochaska W, Lowry D, Klügel A, Hoernle K (2014) Petroleum migration, fluid mixing, and halokinesis as the main ore-forming processes at the peridiapiric Jbel Tirremi fluorite-barite hydrothermal deposit, northeastern Morocco. Econ Geol 109:1223–1256

Bouabdellah M, Niedermann S, Velasco F (2015) The Touissit-Bou Beker Mississippi Valley-type district of northeastern Morocco: relationships to the Messinian salinity crisis, Late Neogene-Quaternary alkaline magmatism, and buoyancy-driven fluid convection. Econ Geol 110:1455–1484

Bouhlel S, Leach DL, Johnson CA, Marsh E, Salmi-Laouar S, Banks DA (2016) A salt diapir-related Mississippi Valley-type deposit: the Bou Jaber Pb-Zn-Ba-F deposit, Tunisia: fluid inclusion and isotope study. Mineral Deposita 51:749–780

Calderón Y, Baby P, Hurtado C, Brusset S (2017a) Thrust tectonics in the Andean retro-foreland basin of northern Peru: Permian inheritances and petroleum implications. Mar Pet Geol 82:238–250. https://doi.org/10.1016/j.marpetgeo.2017.02.009

Calderón Y, Vela Y, Hurtado C, Bolaños R, Baby P, Eude A, Roddaz M, Brusset S, Calvès G (2017b) Petroleum systems restoration of the Huallaga—Marañon Andean Retroforeland Basin, Peru in: AbuAli MA, Moretti I, Bolås HMN (eds) Memoir 114: Petroleum Systems Analysis—Case Studies. AAPG Special Volumes, pp 95-116

Carothers WW, Kharaka YK (1980) Stable carbon isotopes of HCO3− in oil-field waters—implications for the origin of CO2. Geochim Cosmochim Acta 44:323–332

Catchpole H, Kouzmanov K, Fontboté L, Guillong M, Heinrich CA (2011) Fluid evolution in zoned Cordilleran polymetallic veins—insights from microthermometry and LA-ICP-MS of fluid inclusions. Chem Geol 281:293–304

Catchpole H, Kouzmanov K, Bendezú A, Ovtcharova M, Spikings R, Stein H, Fontboté L (2015a) Timing of porphyry (Cu-Mo) and base metal (Zn-Pb-Ag-Cu) mineralisation in a magmatic-hydrothermal system—Morococha district, Peru. Mineral Deposita 50:895–922

Catchpole H, Kouzmanov K, Putlitz B, Seo JH, Fontboté L (2015b) Zoned base metal mineralization in a porphyry system: origin and evolution of mineralizing fluids in the Morococha District, Peru. Econ Geol 110:39–71. https://doi.org/10.2113/econgeo.110.1.39

Charef A, Sheppard SMF (1987) Pb-Zn mineralization associated with diapirism: fluid inclusion and stable isotope (H, C, O) evidence for the origin and evolution of the fluids at Fedj-El-Adoum, Tunisia. Chem Geol 61:113–134

Claypool GE, Holser WT, Kaplan IR, Sakai H, Zak I (1980) The age curves of sulfur and oxygen isotopes in marine sulfate and their mutual interpretation. Chem Geol 28:199–260

Cowan EJ, Beatson RK, Fright WR, McLennan TJ, Mitchell TJ (2002) Rapid geological modelling Applied Structural Geology for Mineral International Symposium. Kalgoorlie, pp 23–25

Cowan EJ, Beatson RK, Ross HJ, Fright WR, McLennan TJ, Evans TR, Carr JC, Lane RG, Bright DV, Gillman AJ (2003) Practical implicit geological modelling Fifth international mining geology conference. Australian Institute of Mining and Metallurgy Bendigo, Victoria, pp. 89–99

de Oliveira SB, Juliani C, Monteiro LVS (2019a) Mineral characterisation of the non-sulphide Zn mineralisation of the Florida Canyon deposit, Bongará District, Northern Peru. Appl Earth Sci 128:27–36. https://doi.org/10.1080/25726838.2018.1556033

de Oliveira SB, Leach DL, Juliani C, Monteiro LVS, Johnson CA (2019b) The Zn–Pb mineralization of Florida Canyon, an evaporite-related Mississippi Valley-type deposit in the Bongará District, Northern Peru. Econ Geol 114:1621–1647. https://doi.org/10.5382/econgeo.4690

de Oliveira SB, Saldanha AA (2019) Application of mineral norm calculation in the resource evaluation of the sulphide and non-sulphide Zn-Pb mineralisation of the Florida Canyon MVT deposit, Peru. Appl Earth Sci 128:96–105. https://doi.org/10.1080/25726838.2019.1619057

de Oliveira SB, Juliani C, Monteiro LVS, Tassinari CCG (2020) Structural control and timing of evaporite-related Mississippi Valley-type Zn–Pb deposits in Pucará Group, Northern Central Peru. J S Am Earth Sci 103:102736

Fontboté L (1990) Stratabound ore deposits in the Pucará basin In: Fontboté L, Amstutz G. C., Cardozo M., Cedillo E, Frutos J (eds) Stratabound Ore Deposits in the Andes. Springer-Verlag, Berlin Heildelberg, pp 253-266

Fontboté L, Gorzawski H (1990) Genesis of the Mississippi Valley-type Zn-Pb deposit of San Vicente, central Peru; geologic and isotopic (Sr, O, C, S, Pb) evidence. Econ Geol 85:1402–1437

Fontboté L, Gunnesch KA, Baumann A (1990) Metal sources in stratabound ore deposits in the Andes (Andean cycle)—lead isotopic constraints in: Fontboté L, Amstutz G. C., Cardozo M., Cedillo E, Frutos J (eds) Stratabound ore deposits in the Andes. Springer-Verlag, Berlin Heildelberg, pp 759-773

Goldstein RH, Reynolds TJ (1994) Systematics of fluid inclusions in diagenetic minerals. SEPM.199

Gunnesch KA, Baumann A (1984) The Atacocha district, central Peru: some metallogenetic aspects Syngenesis and Epigenesis in the Formation of Mineral Deposits. Springer, pp:448–456

Gunnesch KA, Baumann A, Gunnesch M (1990) Lead isotope variations across the central Peruvian Andes. Econ Geol 85:1384–1401

Hoefs J (1980) Stable isotope geochemistry. Springer, Berlin.437

INGEMMET (1999) Mapa geológico del Perú, Escala 1:1,000,000. Instituto Geológico Minero y Metalúrgico. Lima, Peru

Johnson CA, Stricker CA, Gulbransen CA, Emmons MP (2018) Determination of $\delta^{13}C$, $\delta^{15}N$, or $\delta^{34}S$ by isotope-ratio-monitoring mass spectrometry using an elemental analyzer US Geological Survey Techniques and Methods. pp. 20

Kampschulte A, Strauss H (2004) The sulfur isotopic evolution of Phanerozoic seawater based on the analysis of structurally substituted sulfate in carbonates. Chem Geol 204:255–286. https://doi.org/10.1016/j.chemgeo.2003.11.013

Koepnick RB, Denison RE, Burke WH, Hetherington EA, Dahl DA (1990) Construction of the Triassic and Jurassic portion of the Phanerozoic curve of seawater $^{87}Sr/^{86}Sr$. Chemical Geology: Isotope Geoscience section 80:327–349

Korte C, Kozur HW, Bruckschen P, Veizer J (2003) Strontium isotope evolution of Late Permian and Triassic seawater. Geochim Cosmochim Acta 67:47–62

Kouzmanov K, Bendezú A, Catchpole H, Ageneau M, Pérez JA, Fontboté L (2008) The Miocene Morococha district, central Peru: Large-scale epithermal polymetallic overprint on multiple intrusion-centered porphyry systems Australasian Institute of Mining and Metallurgy, Pacific Rim Congress. pp 117-121

Leach DL, Sangster DF (1993) Mississippi Valley-type lead-zinc deposits. Geol Assoc Can Spec Pap 40:289–314

Leach DL, Sangster DF, Kelley KD, Large RR, Garven G, Allen CR, Gutzmer J, Walters S (2005) Sediment-hosted Pb-Zn deposits: a global perspective. Econ Geol 100:561–608

Leach DL, Song Y-C, Hou Z-Q (2017) The world-class Jinding Zn–Pb deposit: ore formation in an evaporite dome, Lanping Basin, Yunnan, China. Mineral Deposita 52:281–296

Leach DL, Song Y (2019) Sediment-hosted zinc-lead and copper deposits in China In: Chang Z, Goldfarb R (eds) Mineral deposits of China. pp 325-409

Machel HG (2001) Bacterial and thermochemical sulfate reduction in diagenetic settings—old and new insights. Sediment Geol 140: 143–175

Mégard F (1968) Geología del cuadrángulo de Huancayo 25-m-[Boletín A 18] INGEMMET Boletín, Serie A: Carta Geológica Nacional. Servicio de Geología y Minería, Lima, p 123

Mégard F (1984) The Andean orogenic period and its major structures in central and northern Peru. J Geol Soc 141:893–900

Mégard F (1987) Structure and evolution of the Peruvian Andes In: Schaer JP, Rodgers J (eds) The Anatomy of Mountain Ranges. Princeton University, Princeton, New Jersey, pp. 179–210

Megaw PKM, Ruiz J, Titley SR (1988) High-temperature, carbonate-hosted Ag-Pb-Zn (Cu) deposits of northern Mexico. Econ Geol 83:1856–1885

Moritz R, Fontboté L, Spangenberg J, Rosas S, Sharp Z, Fontignie D (1996) Sr, C and O isotope systematics in the Pucará basin, central Peru. Mineral Deposita 31:147–162

Noble DC, Silberman ML, Mégard F, Bowman HP (1978) Comendite (peralkaline rhyolite) and basalt in the Mitu Group, Peru: evidence for Permian-Triassic lithospheric extension in the central Andes. US Geological Survey Journal of Research 6:453–457

Ohmoto H, Rye RO (1979) Isotopes of sulfur and carbon. Geochemistry of Hydrothermal Ore Deposits (Barnes, HL, ed.), 509-567. John Wiley & Sons Inc., N Y

Ohmoto H (1986) Stable isotope geochemistry of ore deposits. Rev Mineral 16:491–560

Petit JP (1987) Criteria for the sense of movement on fault surfaces in brittle rocks. Journal of Structural Geology 9:597–608. doi: https://doi.org/10.1016/0191-8141(87)90145-3

Reid CJ (2001) Stratigraphy and mineralization of the Bongara MVT zinc-lead district, northern Peru. University of Toronto, Toronto, p 179

Ritterbush KA, Rosas S, Corsetti FA, Bottjer DJ, West AJ (2015) Andean sponges reveal long-term benthic ecosystem shifts following the end-Triassic mass extinction. Palaeogeogr Palaeoclimatol Palaeoecol 420:193–209. https://doi.org/10.1016/j.palaeo.2014.12.002

Rosas S, Fontboté L, Tankard A (2007) Tectonic evolution and paleogeography of the Mesozoic Pucará Basin, central Peru. J S Am Earth Sci 24:1–24

Rottier B, Kouzmanov K, Casanova V, Bouvier A-S, Baumgartner LP, Wälle M, Fontboté L (2018a) Mineralized breccia clasts: a window into hidden porphyry-type mineralization underlying the epithermal polymetallic deposit of Cerro de Pasco (Peru). Mineral Deposita 53:919–946. https://doi.org/10.1007/s00126-017-0786-9

Rottier B, Kouzmanov K, Casanova V, Wälle M, Fontboté L (2018b) Cyclic dilution of magmatic metal-rich hypersaline fluids by magmatic low-salinity fluid: a major process generating the giant epithermal polymetallic deposit of Cerro de Pasco, Peru. Econ Geol 113:825–856. https://doi.org/10.5382/econgeo.2018.4573

Sánchez A (1995) Geología de los cuadrángulos de Bagua Grande, Jumbilla, Lonya Grande, Chachapoyas, Rioja, Leimebamba y Bolívar: hojas 12-g, 12-h, 13-g, 13-h, 13-i, 14-hy 15-h. Instituto Geológico Minero y Metalúrgico Peru

Schaltegger U, Guex J, Bartolini A, Schoene B, Ovtcharova M (2008) Precise U–Pb age constraints for end-Triassic mass extinction, its correlation to volcanism and Hettangian post-extinction recovery. Earth Planet Sci Lett 267:266–275. https://doi.org/10.1016/j.epsl.2007.11.031

Schütfort EG (2001) The genesis of the San Vicente lead zinc rhythmite deposit, Peru: a petrologic, geochemical, and sulfur isotope study. Oregon State University, p 136

Sempere TPA, Cotrina J (2018) An overlooked giant salt basin in Peru 9th INGEPET. Lima, Peru, p 18

Sillitoe RH (2010) Porphyry copper systems*. Econ Geol 105:3–41. https://doi.org/10.2113/gsecongeo.105.1.3

Soler P, Lara MA (1990) Minor and Trace Elements in the Polymetallic Stratabound Ore Deposits of the Central Peruvian Andes. In: Minor and trace elements in the polymetallic stratabound ore deposits of the Central Peruvian Andes in: Fontboté L, Amstutz GC, Cardozo M, Cedillo E, Frutos J (eds) Stratabound ore deposits in the Andes. Springer, Berlin, pp 735–748

Spangenberg J, Fontboté L, Sharp ZD, Hunziker J (1996) Carbon and oxygen isotope study of hydrothermal carbonates in the zinc-lead deposits of the San Vicente district, central Peru: a quantitative modeling on mixing processes and CO_2 degassing. Chem Geol 133:289–315

Spangenberg JE, Fontboté L, Macko SA (1999) An evaluation of the inorganic and organic geochemistry of the San Vicente Mississippi Valley-type zinc-lead district, central Peru; implications for ore fluid composition, mixing processes, and sulfate reduction. Econ Geol 94:1067–1092

Spikings R, Reitsma MJ, Boekhout F, Mišković A, Ulianov A, Chiaradia M, Gerdes A, Schaltegger U (2016) Characterisation of Triassic rifting in Peru and implications for the early disassembly of western Pangaea. Gondwana Res 35:124–143. https://doi.org/10.1016/j.gr.2016.02.008

Szekely TS, Grose LT (1972) Stratigraphy of the carbonate, black shale, and phosphate of the Pucará Group (Upper Triassic—Lower Jurassic), Central Andes, Peru. Geol Soc Am Bull 83:407–428

Thompson TB, Beaty DW (1990) Geology and the origin of ore deposits in the Leadville District, Colorado: part II. Oxygen, hydrogen, carbon, sulfur, and lead isotope data and development of a genetic model. Carbonate-hosted sulfide deposits of the Central Colorado mineral belt Econ Geol Monog 8:156–179

Tuanama N (2016) Controles geológicos del manto intermedio y su relación con la génesis del yacimiento tipo Mississippi Valley en Shalipayco, Junín, Perú Facultad De Ingeniería Geológica. Minera Metalúrgica Y Geográfica. Universidad Nacional Mayor San Marcos Lima, Peru, p 158

Veizer J, Ala D, Azmy K, Bruckschen P, Buhl D, Bruhn F, Carden GAF, Diener A, Ebneth S, Godderis Y, Jasper T, Korte C, Pawellek F, Podlaha OG, Strauss H (1999) $^{87}Sr/^{86}Sr$, $\delta^{13}C$ and $\delta^{18}O$ evolution of Phanerozoic seawater. Chem Geol 161:59–88

Vollgger SA, Cruden AR, Ailleres L, Cowan EJ (2015) Regional dome evolution and its control on ore-grade distribution: insights from 3D implicit modelling of the Navachab gold deposit, Namibia. Ore Geol Rev 69:268–284. https://doi.org/10.1016/j.oregeorev.2015.02.020

Worden RH, Smalley PC (1996) H2S-producing reactions in deep carbonate gas reservoirs: Khuff Formation, Abu Dhabi. Chemical Geology 133:157–171. doi: https://doi.org/10.1016/S0009-2541(96)00074-5

Wotzlaw J-F, Guex J, Bartolini A, Gallet Y, Krystyn L, McRoberts CA, Taylor D, Schoene B, Schaltegger U (2014) Towards accurate numerical calibration of the Late Triassic: High-precision U-Pb geochronology constraints on the duration of the Rhaetian. Geology 42:571–574. https://doi.org/10.1130/G35612.1

Zheng Y-F (1993) Calculation of oxygen isotope fractionation in hydroxyl-bearing silicates. Earth and Planetary Science Letters 120:247-263. doi: https://doi.org/10.1016/0012-821X(93)90243-3